Chapter 12

Multi-Physical Modeling for IAQ Monitoring

Giuseppe Petrone, Carla Balocco and Giuliano Cammarata

Additional information is available at the end of the chapter

http://dx.doi.org/10.5772/45817

1. Introduction

Indoor air quality (IAQ) is a term referring to the air quality within buildings, relating to the health and comfort of building occupants. During the past decades, a significant effort was spent in order to understand the phenomenological aspects concerning IAQ and its human perception [1, 2]. IAQ can be affected by microbial contaminants (mold, bacteria), gases (including carbon monoxide, radon, volatile organic compounds), particulates, or any mass or energy stressor that can induce adverse health conditions. Using ventilation to dilute contaminants, filtration, and source control are the primary methods for improving indoor air quality in most buildings. Many researchers investigated both experimentally and numerically on IAQ and thermal comfort in specific applications [3-5], that generally depend on ventilation system, building geometry, pollutant source characteristics, thermal and fluid boundary conditions such as flow rate, locations of supply outlets and return inlets, and diffuser characteristics [6]. Usually, indoor CO_2 concentration is monitored in order to estimate the air quality level and to assess the performance of a mechanical ventilation system [7, 8]. Also, CO_2 concentration is often used to estimate building air change rates. Indoor CO_2 concentrations above about 1000 ppm are generally regarded as indicative of ventilation rates that are unacceptable with respect to body odors. On the other hand, concentrations of CO_2 below 1000 ppm do not always guarantee that the ventilation rate is adequate for removal of air pollutants from other indoor sources [9]. Several class of indoor environments could be considered as interesting subject of studies related to the air quality requirements, such as theatres or auditorium halls, cabins of means of transportation and hospital rooms. In theatre or auditorium halls, people sharing the internal atmosphere represent the main CO_2 source. They do not move significantly and CO_2 production is for the most part related to their breathing. This allows to build up or perform detailed experimental set-up or numerical models in terms of internal CO_2 load. Among the investigations dealing with this subject, a recent paper [10] numerically studied how two ventilation systems with the same air inlet arrangement, but different systems of air extraction, affect the air speed, temperature and CO_2 concentration profile inside an

auditorium. It was showed as the lowest rate of air change leads to the increase of temperature. It was found that CO_2 concentration decreases rapidly if the ventilation rate is increased, in this case by the unexpectedly large factor of five. Cheong et al. studied both IAQ [11] and thermal comfort [12] in lecture theatres. The overall results suggested that the ventilation system, in that case a full air-conditioning system, was effective in removing indoor air pollutants and achieving reasonable IAQ. A study proposed by Noh et al. [13] focused on thermal comfort and indoor air quality in a lecture theatre with a 4-way cassette air conditioning and mixing ventilation system. It is showed that increasing the discharge angle from the supply grilles on the cassette unit makes uniformity of thermal comfort worse, but rarely affects IAQ. Recently, Kavgic et al. [14] experimentally monitored and numerically analyzed IAQ and thermal comfort in a theatre hall equipped by a displacement system for ventilation and air conditioning. The paper showed as, for the most part of the monitored period, the environmental parameters were within the standard limits of thermal comfort and IAQ. Otherwise, the calculated ventilation rates showed that the theatre was mostly over-ventilated, with negative consequences for its energy consumption. As above introduced, the bio-effluents diffusion in indoor environments is a very actual issue of interest because of the potential risk of infections transmission between people sharing the same atmosphere. This issue takes also top relevance when considering indoor environment characterized by very high occupant density, such as the cabins of transportation means. In order to avoid high concentration regions of any air pollutant inside the cabins, environmental control system is devoted to dilute the contaminant concentration by introducing fresh air inside. Since cabins have usually more complex geometry and lower outside air supply rate per person as compared to buildings, it is very challenging to design comfortable and healthy cabin environment for transportation means. Among the experimental works concerning this topic, Wang et al. [15] conduced several trials in order to measure the local mean age of air and the ventilation effectiveness factor (VEF) at the breathing level of the passengers. Carbon dioxide was used as the trace gas to determine the local mean age of air and the VEF. The air velocity profiles measured using a volumetric particle tracking velocimetry (VPTV) system were used to generate the airflow patterns and investigate the underlying mechanism affecting the local mean age of air and the VEF. Their results mainly show as the local mean age of air was affected not only by the velocity magnitude, but also by the local airflow patterns such as jet and recirculation. Except for the recirculation regions, the higher mean air velocity corresponded to a lower local mean age of air, indicating a higher net air exchange rate. In the strong air recirculation regions, the higher air velocity did not lead to the lower local mean age of air. This was because the ''old'' air was kept in the recirculation area, and no sufficient freshly supplied air was introduced. The findings of Wang et al. well underlines the importance of carrying-out velocity and pressure distribution maps that are the real important primary indexes in order to investigate on IAQ. Both in buildings and transportation means applications it is recently also arising interest in evaluating air quality and thermal comfort conditions depending on layout-out adopted for air distribution systems [16]. The most common schemes used in HVAC applications are the Mixing Air Distribution (MAD), the Personalized Air Distribution (PAD) and the Under Floor Displacement system (UFD). In

the MAD system, ventilating air is supplied at the ceiling level with a high velocity and then mixes with the air inside the hall. Recovery grids are located at the floor level. The PAD system [17-19] supplies fresh air directly to the breathing area of a person. As it is applied in some movie theatres, diffusers are located on the chair back-side in order to supply fresh air to the person seated on the rear row [20]. In this layout, air is usually recovered at the ceiling level. The functional principle of the UFD system [21] is otherwise based on the buoyancy flow induced close to the human body because of metabolic heat dissipation. Air is supplied at the floor level, close to the heat source. The buoyancy driven upstream flow joins the recovery grids located at the ceiling [22]. In this context it appears more and more interesting to strike a balance among the different scheme based on comparative analyses between different ventilating system layouts in assuring the best air quality and thermal comfort in a chosen application [23]. Let now consider the IAQ in hospitals: because of the risk of infections transmission, the IAQ really assumes a crucial role. This includes both the Isolation Room (IR) and the Operating Theatre (OT). Different engineering standards for the design of operating theatres and Heating Ventilation and Air Conditioning (HVAC) plant system are adopted by several countries. Guidelines and advice are available regarding air quality and how to provide it, as well as other interventions that may reduce the incidence of postoperative infections. The HVAC and IAQ impact on virus and bacteria load, but also aerosol diffusion in the OT has been widely investigated [24, 25]. The risk of virus dispersal and post-operation infections depends mainly on airflow behavior and direction changes caused by people moving or doors opening. In recent years several studies have focused on computational models using fluid dynamics approaches to investigated airflow patterns and the related spreading of infection in isolation and hospitalization rooms and in particular in OTs for different ventilation systems (for example operating under open or closed-door conditions) [26]. The main attention of these papers has been the evaluation of the effects of negative pressure in isolation rooms accommodating patients with highly infectious diseases. Opening the door causes the dispersion of infectious air out of the isolation room. An isolation room held at negative pressure to reduce aerosol escape and a high air-change rate to allow rapid removal of aerosols can eliminate transmission of infectious aerosols to those outside the room. Tunga and collaborators [27] found that an air velocity above 0.2 m/s via a doorway effectively prevents the spread of airborne contaminants out of the isolation room with an open door. In a recent paper the change of an OT from positive to negative pressure environment [28] has been analyzed. Results show that the dispersion pattern of bacteria in the negative pressure theatre were as good as, if not better than, those in the original positive pressure design. Several studies focused on the air flow patterns in the OT, directed to turbulent versus displacement ventilation and laminar air flow systems [29] The laminar airflow (LAF) of OTs is not a strictly accurate description, as it does not fulfill the aerodynamic conditions for genuine laminar flow. Unidirectional or linear airflow is a better alternative, reflecting the actual pattern of air movement in parallel lines. The advantage of using LAF over the turbulent counterpart is its ability to minimize infection by mobilizing a relatively uniform and large volume flow of clean air. After passing through the three stages of filtration (with a HEPA filter as the final stage), the conditioned air enters the OT through a large supply diffuser that usually occupies a substantial ceiling area and

moves towards the surgical area making only a single transit. When the room air moves in a single direction at a sufficient velocity, flow due to heat or movement are abolished and the re-entrainments of particles into the operative field are stopped [30]. When a solid object is encountered, the air flows round the object and the laminar-flow pattern is distorted only in the immediate surroundings of the object. Contaminants are flushed out as soon as they are liberated without migration to other areas. The LAF has two main configurations: vertical and horizontal flow. The selection depends on several factors, including the plane of movements employed in the surgical process, the rate of particle emission, the degree of cleanliness required and its cost-effectiveness. A recent article [31] shows the contamination diffusion in an ISO5 class operating room with vertical LAF when the door is open by a computational fluid dynamic (CFD) simulation. In this last paper, the influence of the door-opening procedure was ignored since the door of the operating room is a sliding one and in particular the effect of people crossing with and without a stretcher is disregarded. Some authors used numerical [32] or experimental [33] approaches to investigate the effects of one moving person or the movement of a sliding door on the air distribution, including air velocity and pressure field but also CO_2 contaminant distribution, within generic ventilated or specific negative pressure isolation rooms [34]. Among the numerical based studies, simulation of object or person movements has been handled directly or indirectly [35]. Direct simulation includes the real movement of the real "object" inside the solution domain and requires a moving mesh approach in order to be realized. One of the most recent methods used for this kind of application is the so-called Arbitrary Lagrangian-Eulerian (ALE) method, in certain cases allowing resolution of the limit of small distortions allowed in the numerical model by the traditional Lagrangian approach. However, the direct simulation of the moving object requires very expensive computational cost. They are related on the one hand to the degrees of freedom increasing for a chosen number on mesh nodes, and on the other to the remeshing procedure, often needed during computations. The basic principle of the indirect simulation of a moving object in surrounding air consists otherwise in keeping into account the effects of the object's movement on the air flow. Two indirect numerical procedures were recently tested and applied by Brohus et al. [36] in order to simulate the effect of the surgical staff movements on contaminant concentration in an operating room. In this framework, this chapter presents a collection of results obtained by several numerical models built-up in order to investigate on IAQ basing on real-world scenarios and events. In particular, they refer to critical applications, characterized by high people density (movie theatre hall, cabins of means of transportation) or contamination risk (hospital rooms). The case studies presented in the following are introduced by a brief description of the applied mathematical and numerical models.

2. Numerical modelling

2.1. Continuous equations

Numerical models presented in this chapter have been built in COMSOL Multiphysics v.3.5a, a commercial FEM based software widely used for solving multi-physical problems governed by coupled ordinary and partial differential equations. The multi-physical problems involve at least solution of mass, momentum, energy conservation laws. Under

assumptions of Newtonian fluid and uncompressible turbulent flow, the Reynolds Averaged Navier-Stokes equations read as in following:

$$\rho\frac{\partial \mathbf{U}}{\partial t}+\rho\left(\mathbf{U}\cdot\nabla\right)\mathbf{U}=\nabla\cdot\left[-p\mathbf{I}+\left(\mu+\mu_T\right)\left(\nabla\mathbf{U}+\left(\nabla\mathbf{U}\right)^{\mathrm{T}}\right)\right]+F \tag{1}$$

$$\nabla\cdot\mathbf{U}=0 \tag{2}$$

$$\rho\frac{\partial k}{\partial t}+\rho\mathbf{U}\cdot\nabla k=\nabla\cdot\left[\left(\mu+\frac{\mu_T}{\sigma_k}\right)\nabla k\right]+\frac{1}{2}\mu_T\left[\nabla\mathbf{U}+\left(\nabla\mathbf{U}\right)^{\mathrm{T}}\right]^2-\rho\varepsilon \tag{3}$$

$$\rho\frac{\partial \varepsilon}{\partial t}+\rho\mathbf{U}\cdot\nabla\varepsilon=\nabla\cdot\left[\left(\mu+\frac{\mu_T}{\sigma_\varepsilon}\right)\nabla\varepsilon\right]+\frac{1}{2}C_{\varepsilon 1}\frac{\varepsilon}{k}\mu_T\left[\nabla\mathbf{U}+\left(\nabla\mathbf{U}\right)^{\mathrm{T}}\right]^2-\rho C_{\varepsilon 2}\frac{\varepsilon^2}{k} \tag{4}$$

$$\rho C_p\frac{\partial T}{\partial t}+\rho C_p\mathbf{U}\cdot\nabla T=\nabla\cdot\left(\lambda\nabla T\right)+Q \tag{5}$$

Where $\mu_T = \rho C_\mu k^2/\varepsilon$ represents the turbulent viscosity. Values adopted for constants appearing in the above equations are determined from experimental data and reported in Table 1 [37].

C_μ	$C_{\varepsilon 1}$	$C_{\varepsilon 2}$	σ_k	σ_ε
0.09	1.44	1.92	1.0	1.3

Table 1. Numerical values of constants appearing in the adopted mathematical model.

Conservation laws (1-5) used to solve thermal and fluid-dynamical analyses have been coupled in same of applications presented in the following with two specific transport-diffusion equations, whereof the dependent variables are the temperature (solved both in fluid and solid domains), the carbon dioxide concentration and the mean age of air [38, 39], that quantifies the average lifetime of air at a particular location and so gives an indication of the air "freshness":

$$\frac{\partial CO_2}{\partial t}+\mathbf{U}\cdot\nabla CO_2=D\nabla^2 CO_2 \tag{6}$$

$$\rho\frac{\partial \tau}{\partial t}+\rho\mathbf{U}\cdot\nabla\tau=\Gamma\nabla^2\tau \tag{7}$$

In the previous equations D and Γ are the diffusion coefficients of carbon dioxide in air and the diffusion coefficient of τ in the air mixture, respectively. Boundary conditions considered for models presented in the following are summarized in Table 2. Logarithmic wall functions were applied in the near wall flow, that has been considered parallel to the wall and being in a wall offset δ_w equal to one half of the boundary mesh element dimension. The equivalent wall

offset in viscous unit is defined as $\delta_w^+ = \delta_w \rho U_\tau / \mu$, being U_τ the frictional velocity. Assumed values for the constant C^+ is 5.5, while the Karman's constant value was set equal to 0.42. Under the general assumption of fully turbulent flow, a turbulent length scale of 0.01 m and a 5% of turbulent intensity were applied at the generic air inlet sections.

Equation	Boundary condition	
(1-2)	Inlet	Symmetry
	$\mathbf{U} = -U_{in}\mathbf{n}$	$\mathbf{n}\cdot\mathbf{U} = 0$ $\mathbf{t}\cdot\left[-p\mathbf{I} + \left(\mu+\mu_T\right)\left(\nabla\mathbf{U} + \left(\nabla\mathbf{U}\right)^{\mathrm{T}}\right)\right]\mathbf{n} = 0$
	Output	Open
	$\left[\left(\mu+\mu_T\right)\left(\nabla\mathbf{U} + \left(\nabla\mathbf{U}\right)^{\mathrm{T}}\right)\right]\mathbf{n} = 0$ $p = p_{out}$	$\left[-p\mathbf{I} + \left(\mu+\mu_T\right)\left(\nabla\mathbf{U} + \left(\nabla\mathbf{U}\right)^{\mathrm{T}}\right)\right]\mathbf{n} = 0$
	Wall	
	$\mathbf{n}\cdot\mathbf{U} = 0$ $\left[\left(\mu+\mu_T\right)\left(\nabla\mathbf{U} + \left(\nabla\mathbf{U}\right)^{\mathrm{T}}\right)\right]\mathbf{n} = \left[\rho C_\mu^{0.25} k^{0.5} / \left(\ln\left(\delta_w^+\right)/\kappa + C^+\right)\right]\mathbf{U}$	
(3)	Inlet	Symmetry
	$k = 3/2\left(I_T U_{in}\right)^2$	$\mathbf{n}\cdot\left[\left(\mu+\mu_k/\sigma_k\right)\nabla k - \rho\mathbf{U}k\right] = 0$
	Output / Open	Wall
	$\mathbf{n}\cdot\nabla k = 0$	$\mathbf{n}\cdot\nabla k = 0$
(4)	Inlet	Symmetry
	$\varepsilon = C_\mu^{0.75}\left(3/2\left(I_T U_{in}\right)^2\right)^{1.5} / L_T$	$\mathbf{n}\cdot\left[\left(\mu+\mu_T/\sigma_\varepsilon\right)\nabla\varepsilon - \rho\mathbf{U}\varepsilon\right] = 0$
	Output / Open	Wall
	$\mathbf{n}\cdot\nabla\varepsilon = 0$	$\varepsilon = \rho C_\mu k^2 / \left(\kappa\delta_w^+\mu\right)$
(5)	Inlet	Symmetry / Insulation
	$T = T_{in}$	$\mathbf{n}\cdot\left(\lambda\nabla T\right) = 0$
	Output	Dispersion
	$\mathbf{n}\cdot\left(\lambda\nabla T\right) = 0$	$\mathbf{n}\cdot\left(\lambda\nabla T\right) = h_{conv}\left(T_{ext} - T\right)$
(6)	Inlet	Interface (fluid/solid)
	$CO_2 = CO_{2in}$	$\mathbf{n}\cdot\left(D\nabla CO_2 + CO_2\mathbf{U}\right) = 0$
	Output/Open	Walls
	$\mathbf{n}\cdot\left(D\nabla CO_2\right) = 0$	$\mathbf{n}\cdot\left(D\nabla CO_2 + CO_2\mathbf{U}\right) = 0$
(7)	Inlet	Interface (fluid/solid)
	$\tau = 0$	$\mathbf{n}\cdot\left(\Gamma\nabla\tau + \tau\mathbf{U}\right) = 0$
	Output/Open	Walls
	$\mathbf{n}\cdot\left(\Gamma\nabla\tau\right) = 0$	$\mathbf{n}\cdot\left(\Gamma\nabla\tau + \tau\mathbf{U}\right) = 0$

Table 2. Numerical values of constants appearing in the adopted mathematical model.

2.2. Numerical methods

Continuous equations have been spatially discretized by a Finite Element approach based on the Galerkin method on non-uniform and non-structured computational grids made of tetrahedral Lagrange second order elements. For each application presented below, influence of spatial discretization has been preliminary studied in order to assure mesh-independent results. In order to prevent rising and propagation of numerical instabilities, an artificial streamline diffusion technique, based on the Galerkin Least-Squared (GLS) method, was employed in simulations. It should be noted that the GLS is a consistent method, which means that it does not perturb the original transport equation. Steady solutions were carried-out by applying an iterative dumped Newton-Raphson scheme [40], classically based on the discretized PDE linearization by a first-order Taylor expansion. An iterative approximation $s^{(k+1)}$ of the steady state s_0 is performed by solving the following system:

$$\begin{cases} J_E\left[\mathbf{S}^{(k)}\right]\delta\mathbf{S}^{(k+1)} = -E\left[\mathbf{S}^{(k)}\right] \\ \delta\mathbf{S}^{(k+1)} = \mathbf{S}^{(k)} + \tilde{\lambda}\ \delta\mathbf{S}^{(k+1)} \end{cases} \tag{8}$$

where $E\left[\mathbf{S}^{(k)}\right]$ is the residual at the k-step, $0 < \tilde{\lambda} \le 1$ is a dumping factor used in calculating the perturbation in the Newton system and the Jacobian operator J_E consists in the difference between perturbed and not perturbed equations linearized at the specific linearization state $\mathbf{S}^{(k)}$. Once $\mathbf{S}^{(k+1)}$ evaluated, the relative error $\Lambda^{(k+1)}$ is computed as:

$$J_E\left[\mathbf{S}^{(k)}\right]\Lambda^{(k+1)} = -E\left[\mathbf{S}^{(k+1)}\right] \tag{9}$$

If $\Lambda^{(k+1)} > \Lambda^{(k)}$, the dumping factor value is reduced and the approximate solution $\mathbf{S}^{(k+1)}$ is computed again, until the relative error is less than its value in the previous step or it underflows a given minimum value, that means solution is not converged. If a successful approximated solution is taken, algorithm proceeds to a next Newton iteration. The iterative procedure ends when the chosen converge criterion is satisfied. Time integration of governing equations has been otherwise performed applying an Implicit Differential-Algebraic (IDA) solver [41], which uses variable-order and variable-step-size Backward Differentiation Formulas (BDF). Because the time-marching scheme is implicit, a nonlinear system of equations must be solved each time step. The previously discussed solving procedure, based on the Newton algorithm, has been exploited to solve this nonlinear system of equations. Algebraic systems of equations coming from differential operator discretization were solved both by a PARDISO package, a direct, high-performance, robust, memory efficient package for solving large sparse unsymmetrical linear systems of equations on shared-memory and distributed-memory multiprocessors.

3. Case studies

3.1. Movie theatre hall: Influence of the air-distribution layout on IAQ and thermal comfort

This case study concerns a movie theatre hall, whose geometry is outlined in Figure 1. The mean goal of this analysis consists in investigating the IAQ depending on the adopted layout for ventilation air distribution inside the indoor environment: Mixing Air Distribution (MAD), Personalized Air Distribution (PAD) and Under Floor Displacement (UFD). The internal dimensions of the hall are 18.5 m in length, 10 m in width and a maximum height of 9 m. The hall disposes of 10 rows of seats and 12 seats per row. Exploiting the room symmetry, a two-dimensional approximation was retained in simulations in order to save computational resources. Geometrical elements have been designed in order to simulate chairs (green) and human bodies (gray) as numerical domains in the considered transversal mid-section of the hall. The main region of the geometry is filled by air (cyan). Specific geometrical boundaries, located at the ceiling level, at the chair rear-side and at the floor level (close to the occupant's feet), have been represented to simulate diffusers and recovery grids for ventilating air. Some details concerning inlet/outflow sections for each ventilation layout analyzed are reported in enlargements of Figure 1. Results are mainly presented in by pictures reporting fluid-dynamical and thermal fields and CO_2 computed levels. Firstly, global fluid-dynamical and thermal results related to the steady solution of the considered systems are presented. Then, air quality is investigated by analyzing the results coming from the transient analyses simulating the human breathing. Finally, a brief discussion of results concerning their comparison with some data available in literature is reported.

3.1.1. Fluid-dynamics and thermal behavior in steady conditions

In Figure 2 air velocity vectors are presented in a color-scaled map identifying their magnitude, for MAD, PAD and UFD system, respectively. Figure 3 reports the corresponding thermal fields. The significant differences in air flow patterns can be appreciated from a distribution system to another.

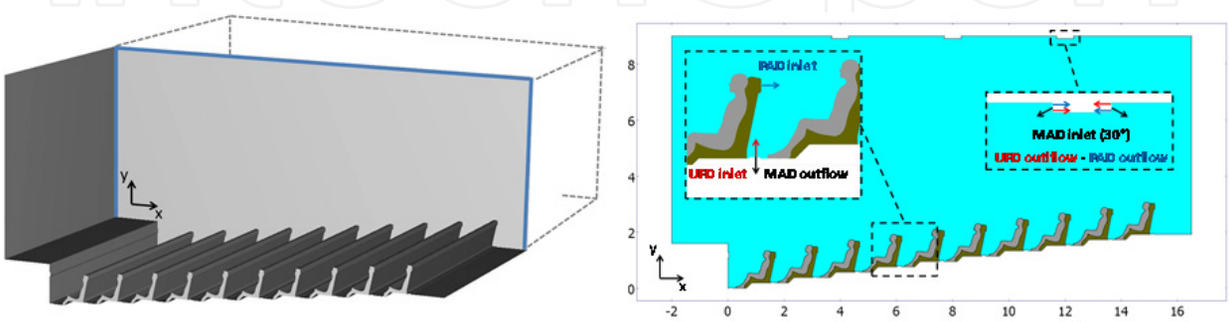

Figure 1. Geometry of the physical system and enlargements reporting details concerning the inlet/outflow sections for each ventilation layout.

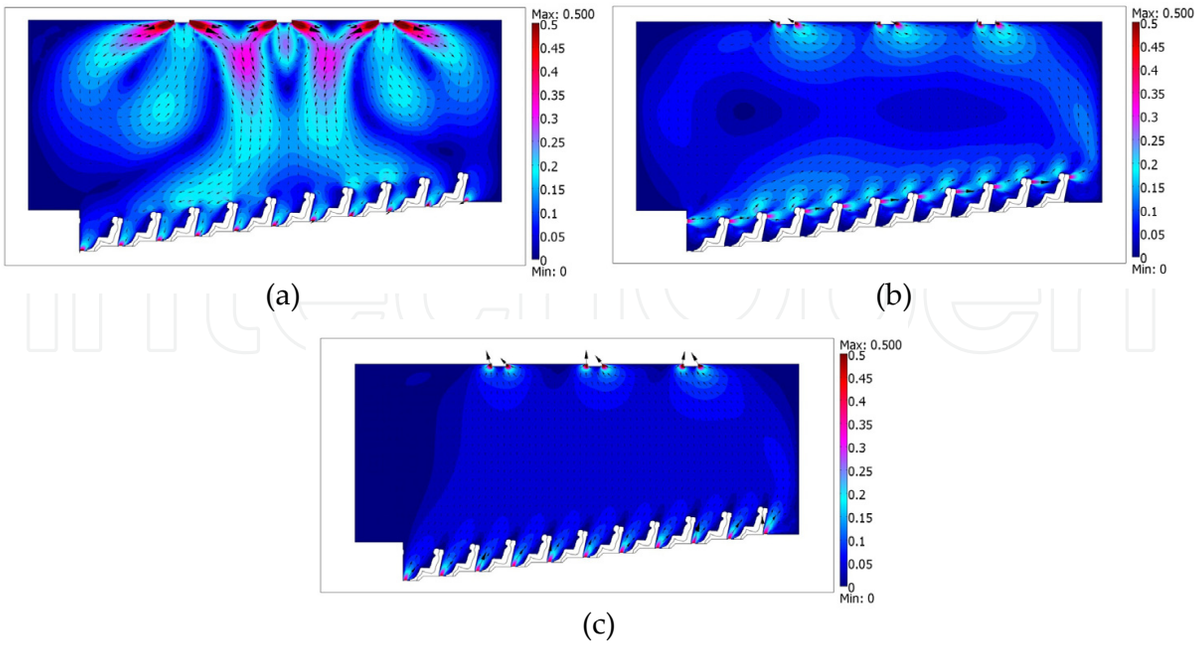

Figure 2. Velocity vectors and velocity magnitude [m/s] for MAD (a), PAD (b) and UFD (c) systems.

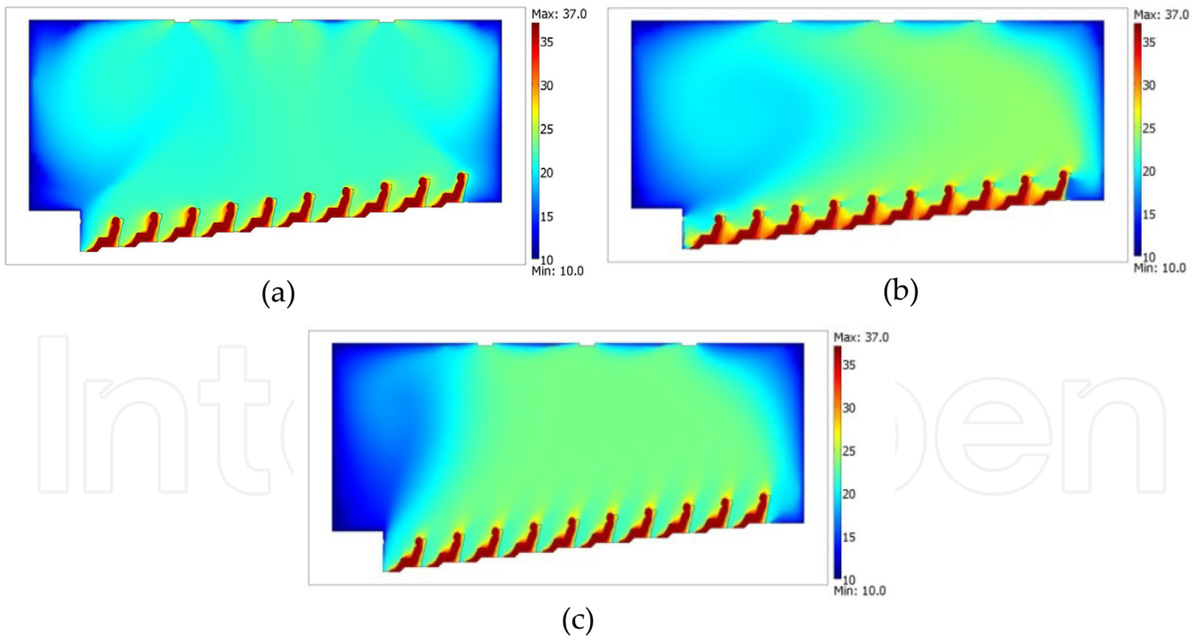

Figure 3. Temperature [°C] distribution for MAD (a), PAD (b) and UFD (c) systems.

Diffusers at the ceiling level determinate in the MAD system an important air circulation in the whole hall, characterized by two main cells located in the headroom close to the stage and the back side of the theatre hall. Otherwise, the intermediate rows of seats appear more

subjected by the ventilating effect. Magnitude of air velocity close to some of people heads (rows 3-4 and 7-8) reaches values of 0.15-0.18 m/s, that is usually considered as a threshold inducing a disagreeable draught effect if exceeded [42]. That condition instead occurs for all the spectators when the PAD system is applied. Ventilating air, supplied by the back chair diffusers, flows too fast (up to 0.2 m/s) in proximity of the spectators' heads. The main air stream is blown to the rear wall of the theatre hall, then air flows up and it is recovered at the ceiling level. This allows almost stagnant conditions close to the stage as well as in the central portion of the hall. In UFD system, velocity of air in the occupied zone appears lower, globally assuring a better comfort condition from this point of view. The stage zone is stagnant.

Thermal fields well highlight the convective heat transfer induced by the fluid flow in the different cases. The average temperature of air for the MAD (20.7 °C) and UFD (20.8 °C) systems appears slightly lower than the PAD one (21.2 °C). However, when PAD system is simulated a high gradient of air temperature is remarked in proximity of each seated person. This is due to the stagnant conditions occurring in region between the chair back and the person legs: very slow velocity of air determinates an "ineffectiveness" in thermal dissipation of the metabolic heat. In that condition the PAD system appears the worse one referring to spectators thermal comfort. However, it is to notice as three-dimensional simulations are needed in order to clarify this aspect. In UFD system thermal plumes upon people heads are evident. In comparison with the MAD, the displacement ventilating system allows to get a much more homogeneous temperature distribution for people seated in the first and late row of seats also. As outlined, all simulated layouts do not assure thermal comfort conditions in the stage region.

3.1.2. Transient analyses and air quality

Transient analyses simulating human breathing have been carried out in order to investigate on air quality inside the movie theatre. CO_2 concentration in indoor air has been considered as an index of overall ventilation adequacy. The human breathing determinates periodical mass flux rate incoming the indoor environment. As a consequence, CO_2 concentration of fresh air (350 ppm) is locally modified. Depending on ventilating layout, the air streams transport differently the bio-effluent inside the hall. Figure 4 report the evaluated maps of CO_2 concentration for MAD, PAD and UFD close to one of occupants. Snapshots refer to 4 time-steps during a breathing period, that was considered occurring in 4 seconds.

Those pictures well elucidate the effect of the periodic function applied for breathing simulation. By adopting the local CO_2 level as index of effectiveness for the air distribution system, the best one seems to be the PAD layout. In fact, it assures a good dilution of the bio-effluent breathed out by the spectators, determining lower concentration of it close to the occupants' faces. On the other hand, the UFD system is characterized by almost stagnant condition in that region, so that extended zones presenting high levels of CO_2 are detected.

The MAD system determinates intermediate conditions from the previous ones. As previously introduced, in order to investigate on the average lifetime of air at a particular location, and giving an indication of the air "freshness", the additional transport-diffusion equation (7) has been also integrated during transient analyses. The "mean age of air" τ [s] has been computed for the studied ventilating layouts. As attended, starting from an arbitrary initial condition, each ventilating system assures, once a given time elapsed, the mean age of air becomes constant. The time range needed to assure that condition is shown to be different from a system to another. The UFD system achieves a τ stationary behavior exceeding 300 seconds about, while that threshold increases for MAD (1000 seconds about) and PAD (1400 seconds about) systems. This different behavior is also highlighted by Figure 5, where the computed mean age of air, evaluated for t=3600 seconds, is plotted in color-scaled maps overall the air volume for the investigated systems. In a MAD layout, air supplied by the ceiling located diffusers has to cover a long path before getting the occupied zone of the theatre hall. As a consequence, audience receive air 100-250 seconds "old" depending on specific place (spectators seated in the intermediate rows take advantage from this point of view). Different conditions occur when supplying air by PAD and UFD systems. Ventilating air is directly introduced by diffusers in the occupied zone, so that the mean age of air close to the people's face results globally lower than 50 seconds for the PAD system (except the first and the second row) and lower than 30 seconds for the UFD system.

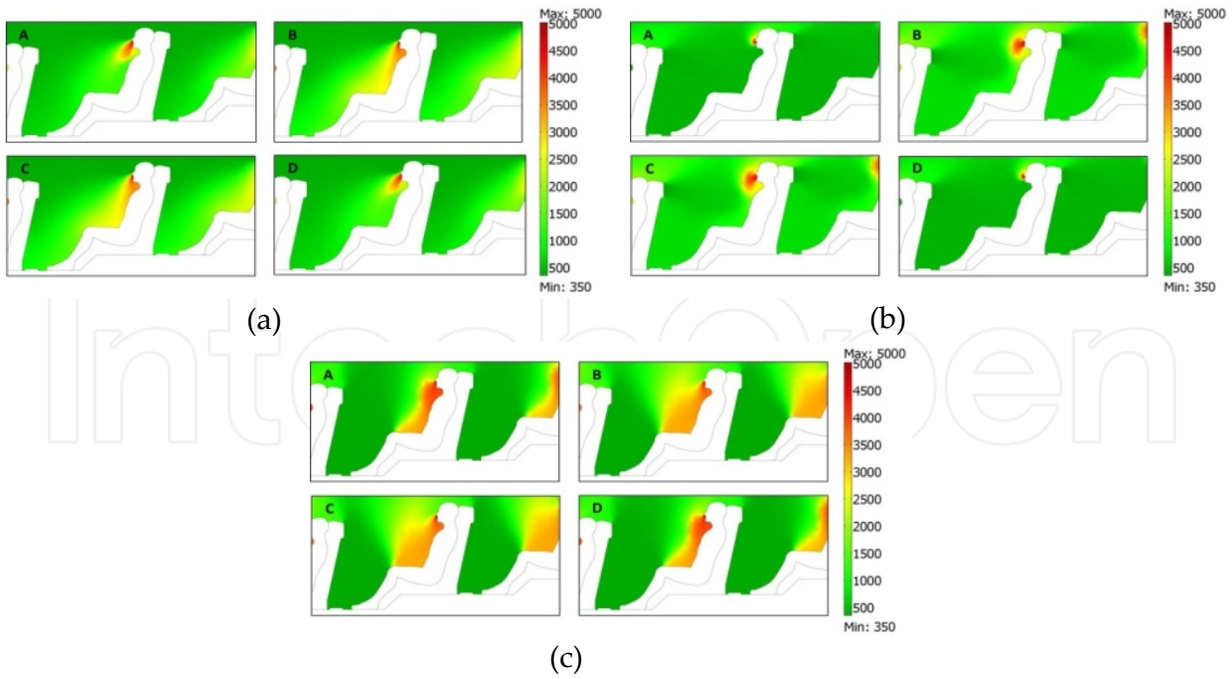

Figure 4. CO_2 concentration map [ppm] close to a person at 4 time steps of a breathing period (t=0 s (A), t=1 s (B), t=2 s (C), t=3 s (D)) for MAD (a), PAD (b) and UFD (c) systems.

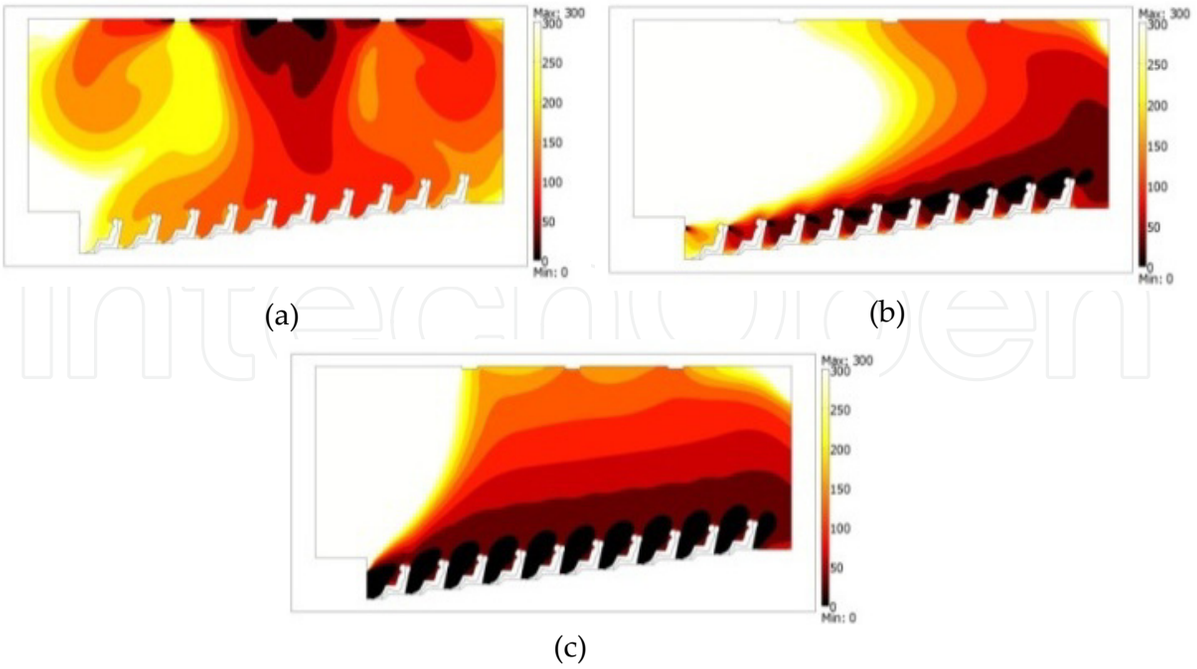

Figure 5. Distribution of the "mean age of air" for MAD (a), PAD (b) and UFD (c) systems.

3.2. Cabins of transportation means: influence of the air-distribution layout on IAQ and thermal comfort

This second case study deals with an investigation on bio-effluents transport and diffusion in ventilated cabins of transportation means and thermal comfort for passengers. As for the previously discussed application, different layouts for ventilation system (MAD, UFD, PAD) are preliminary analyzed in order to strike a balance between air quality degradation and comfort conditions for passengers. Firstly, a simplified geometry consisting in a 2D representation of 5 rows of seats standing inside a cabin was considered (Figure 6), then a more detailed 3D system was investigated in order to further optimize thermal and fluid-dynamical conditions for passengers. Depending on the air distribution system, small differences can be remarked in model geometries: as an instance, the geometrical elements used as inlet and outlet sections for fluid flowing the control volume. Geometrical elements are designed also in order to represent seated human occupants inside the cabin.

Physical properties of fluid are considered constant, except for density in the buoyancy term of the Navier-Stokes equations. Periodic functions has been used as boundary conditions to simulate the human breathing of occupants during time and the relative mass rate of carbon dioxide introduced in the cabin. Referring to the inlet velocity function, it is evaluated considering: the mass rate of air inhaled by a standard person every breathe, the air density, the surface of the nose holes and the breathing frequency. The carbon dioxide mass rate incoming in the control volume is as well computed following the same analytic procedure. In this case the concentration flux is evaluated considering the CO_2 molecular mass and the

rate of CO_2 contained in air breathed out. In order to simulate more real conditions it is supposed that passengers breathe not in phase each other. The phase displacement is imposed in 0.2 second for each passenger.

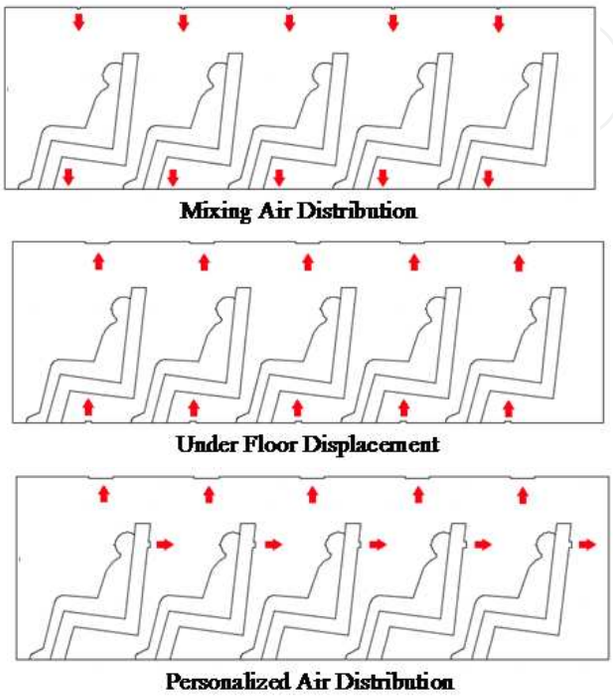

Figure 6. Outline of the cabin for the different layouts of the ventilating system.

3.2.1. Simplified geometry

The obtained results for the simplified 2D geometry are presented in this subsection. Figure 7 shows the velocity field at time instant t=120 [s] for the MAD, UFD and PAD air distribution systems. The significant differences in flow patterns can be appreciated from a distribution system to another. It is to remark the relative difference in the air velocity magnitude occurring close to the passenger faces. While the MAD and UFD systems assure magnitude of velocity lower than 0.15 m/s, the PAD system application determinates values comprised between 0.3-0.4 m/s. This represents the threshold value of induced discomfort in passengers due to a potential air draft perception. In Figure 8 CO_2 concentration maps are plotted for each air distribution system and at different time steps. Because of it is assumed a breathing frequency of 0.25 Hz, images (captured in the range 60-63 seconds) describe the concentration of bio-effluent during a complete breathing act close to the passenger's face. It can be observed as, from the air quality point of view, the best air distribution system appears the PAD one. In fact, it assures a good dilution of the bio-effluent breathed out by the passengers, determining very low concentration of it close to the occupant's nose. On the

other hand, the UFD system is characterized by almost stagnant condition in that region, so that high levels of CO_2 are detected. The MAD system determinates intermediate conditions from the previous ones.

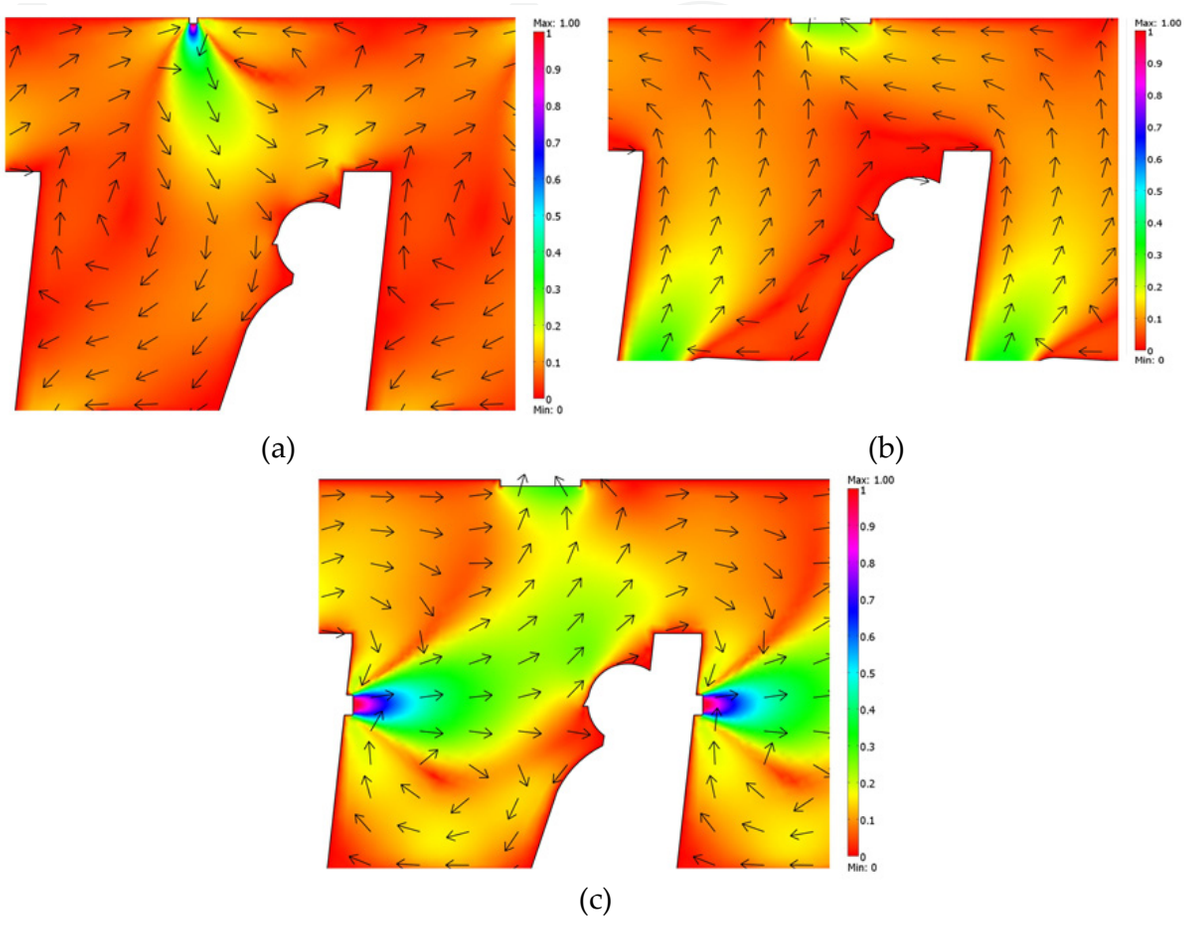

Figure 7. Velocity field [m/s]: MAD (a), UFD (b) and PAD (c) system.

Focalizing now the attention on the potential contamination risk inside the cabin, Figure 9 shows the tracing obtained by monitoring the path of a particle introduced, at the initial time of simulation, close to the nose of the passenger seated in the third row. This kind of post-processing allows to well understand the transport effect on a small mass generated by the fluid flow. Some remarks need to be pointed out. For each air distribution system, the particle path follows the streamlines of air flow. In MAD system, fresh air coming from the cabin ceiling blows the particle down as far as the recovery grids arranged on the floor. The time needed is 23 about seconds. In UFD system, fresh air coming from the bottom push up the particle as far as the grids, this time located on the roof. The time needed is about 24 seconds. In the PAD system, fresh air blown by the seat in front of the breathing passenger let his bio-effluent flow toward the passenger lodged in the rear row. The particle is then

blown toward the outlet section by the rear air jet. The time needed is about 10 seconds. Results mainly show as from the comfort condition the most appropriate system is the UFD system. In fact it assure the lower velocity level close to the passenger's face. From the air quality point of view, the PAD system represent instead the best choice because it allows very low level of stagnant bio-effluent close to the passenger's nose. Anyway, referring to the contamination risk inside the cabin, this system is detected to be the most critical because it allows particle breathed out by a passenger to be potentially inhaled by another. Globally it appears that in absence of relevant challenges to be pursued in the most recent UFD and PAD systems, the classical MAD represent the better compromise between opposite requirements.

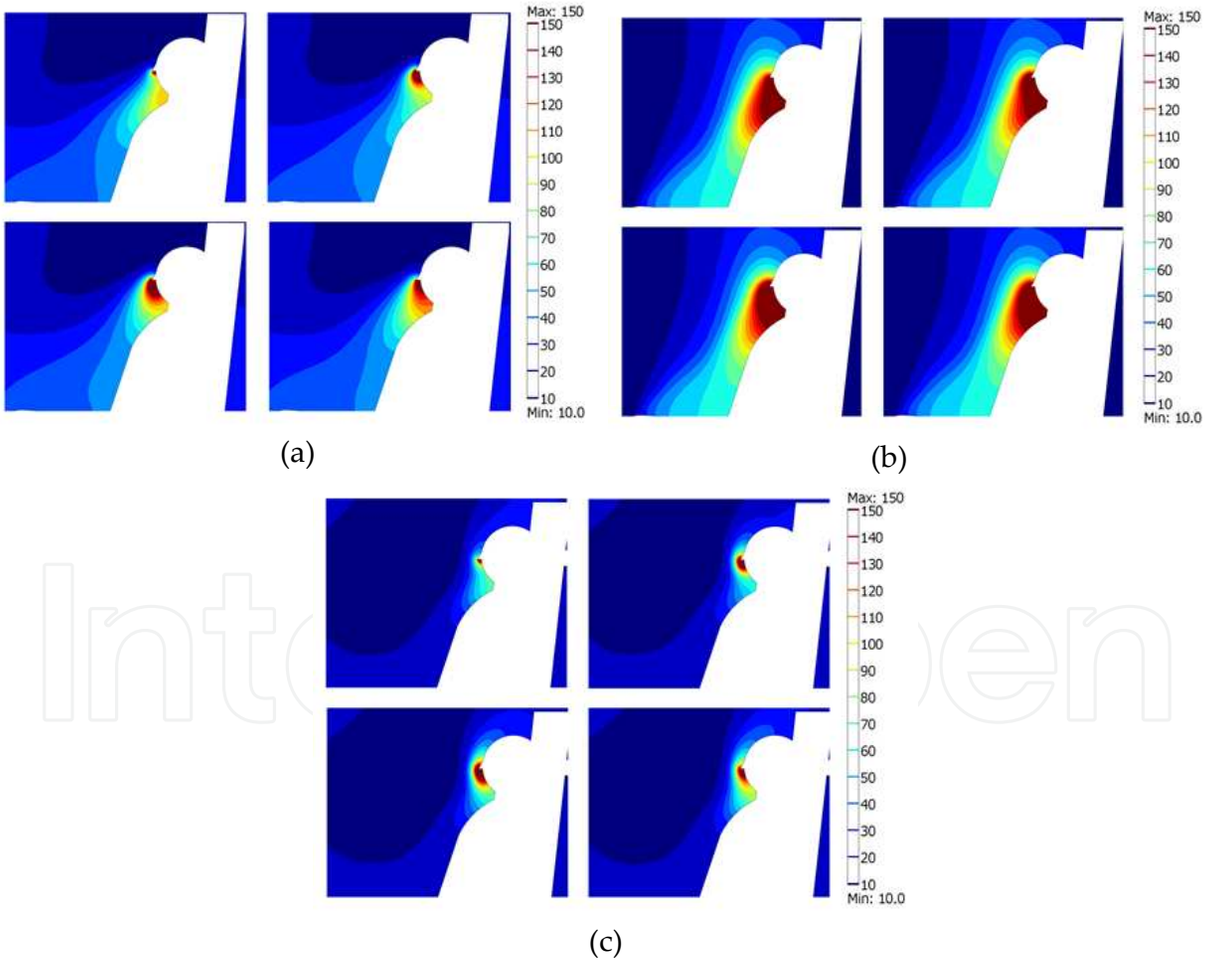

Figure 8. CO_2 levels [mol/m^3] in a breathing cycle for MAD (a), UFD (b) and PAD (c) system.

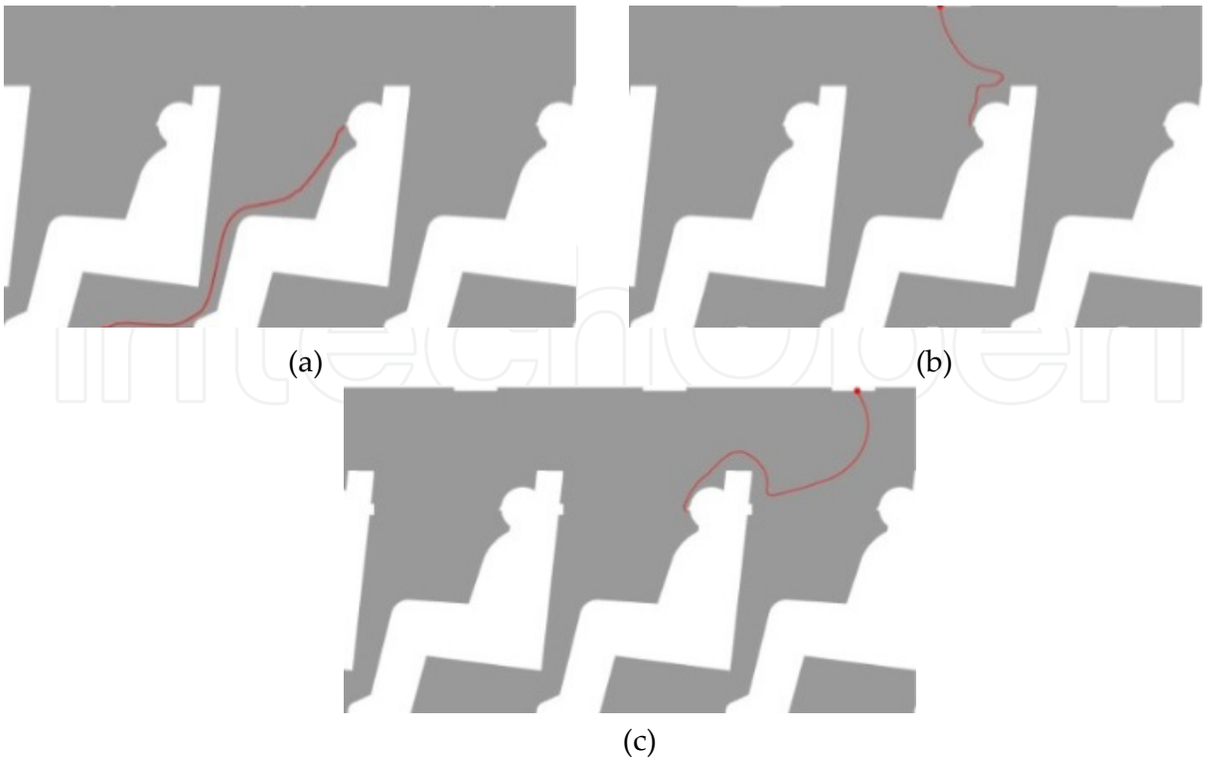

Figure 9. Particle tracing for MAD ((a), final time of processing t=23[s]), UFD ((b), final time of processing t=24[s]), PAD ((a), final time of processing t=10[s]) .

3.2.2. Detailed geometry

The detailed 3D geometry of the system consists in a shorter portion of the cabin, containing two rows of seats. Exploiting the longitudinal symmetry of the cabin, just one half of it has been reproduced. Two inlet sections for fresh air are considered: the first one, located at the roof and representative of a ceiling MAD, is made of rectangular slots positioned in the horizontal channel developing along the cabin aisle; the second one, representative of a UFD ventilation system, is located in correspondence of the lateral side of each seat. Results have been carried-out for the two operating layouts: firstly a pure ceiling system for air inlet is studied, then a second scheme has been considered: inlet sections for conditioning air are also arranged in correspondence of the lateral side of each passenger seat. This layout is representative of a combination between the standard ceiling system and a displacement air distribution system. Both configurations are studied for winter conditions, referring to an external temperature of 5°C. Figure 10 presents isosurfaces of velocity for the first analysed configuration. Ventilation air is provided by four rectangular slots located at the roof in correspondence of the aisle of the bus cabin. The interest was firstly focused on verifying passengers comfort referring to the motion field of ventilation air. In fact it is recognized that values of air velocity exceeding 0.8 m/s could be responsible of discomfort condition for human occupants of a ventilated ambient. Figure 11 shows distribution of air velocity and velocity vectors plotted in a transversal section of the cabin chosen as indicative for verifying comfort of passenger (the surface crosses passengers head). From analysis of Figure 11 it can be verified as the ceiling system for air distribution does not involve in

discomfort for passengers. The inlet velocity for incoming air was chosen at value 2.5 m/s, that well fits with reasonable values usually adopted for this kind of ventilation system . The above discussed consideration is also confirmed by results reported in Figure 12. That figure reports the velocity field in a horizontal transversal section of the cabin. Maximum value of air velocity is reached in a zone not occupied, such as the cabin aisle. From a fluid-dynamical point of view, the second element that could determinate disagreeable condition for occupants is the turbulence level. In Figure 13 streamlines of the vorticity function for the obtained air flow have been reported. From analysis of that finding it is possible to deduce as high turbulence levels only occur in the top portion of the cabin space, so that passengers do not result affected by this potential cause of discomfort. Let now examine the ceiling air distribution system from a thermal point of view. Heating air is introduced from the lateral side of the passenger's seat close to the cabin aisle. On the other hand, the higher level of heat dissipation occurs on the opposite side, close to lateral wall of the bus cabin. This wall obviously confines with the external ambient. Moreover, it is partially made of the window glass characterized by a high thermal conductivity. These assumptions let guess to results obtained from thermal analysis of this inlet layout for heating air.

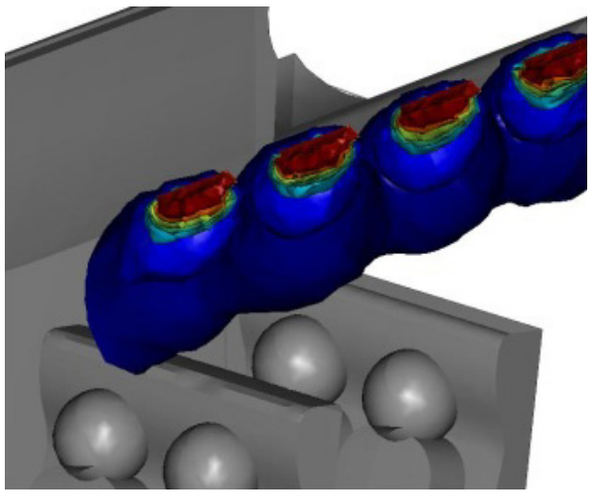

Figure 10. Isosurfaces of velocity.

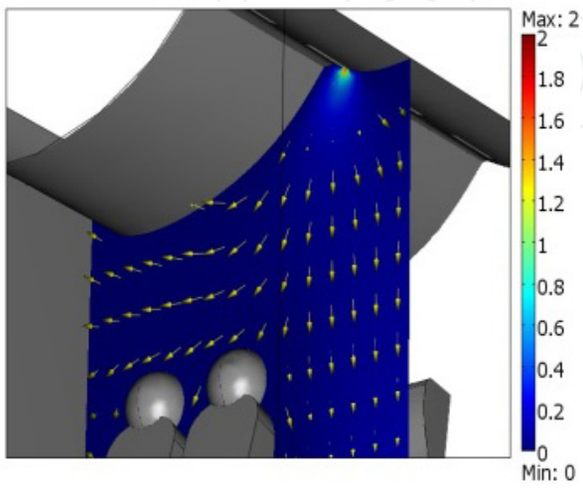

Figure 11. Motion field of air.

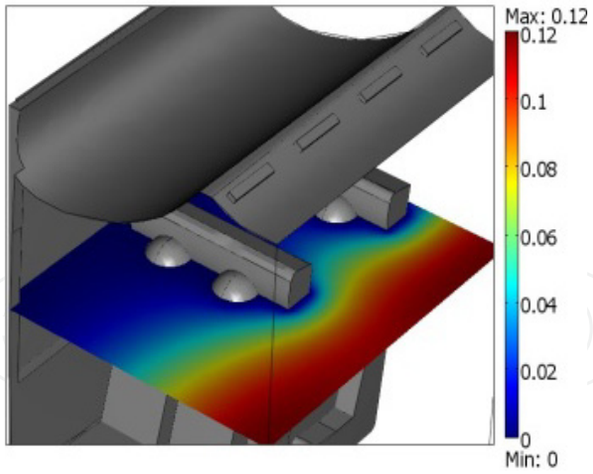

Figure 12. Velocity field.

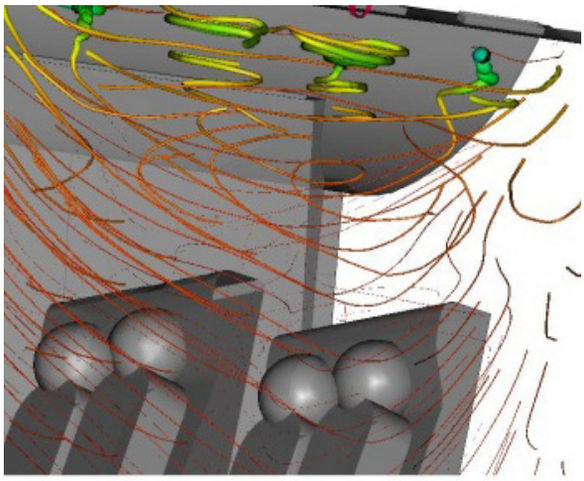

Figure 13. Streamlines of the vorticity function.

In Figure 14 temperature distribution has been plotted on contours of solid elements of the numerical model. Results reported in that figure well show the ineffectiveness of the ceiling air distribution system from a thermal point of view. As previously mentioned, thermal comfort highly depends on uniform distribution of the air temperature surrounding the human body. From Figure 14 is clearly observable as passengers seated close to the window are submitted to strong temperature gradient in horizontal direction. The obtained thermal field does not assure thermal comfort for passengers. Because of that reason it was simulated a second scheme for heating air incoming. As yet mentioned, this second outline of the numerical model takes its inspiration from the displacement air conditioning systems. In order to test this layout of inlet section location, heating air was considered to enter the computational domain in trough out the lateral bottom side of each passengers seat. Figure 15 presents the obtained results. As observable thermal field at solid-fluid interfaces of the numerical model show an almost uniform distribution of temperature in correspondence of the human occupants. That clearly means better comfort conditions for passengers.

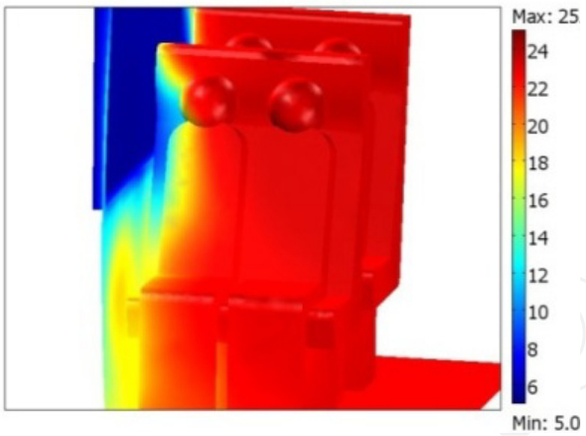

Figure 14. Temperature field at solid-fluid interfaces (MAD).

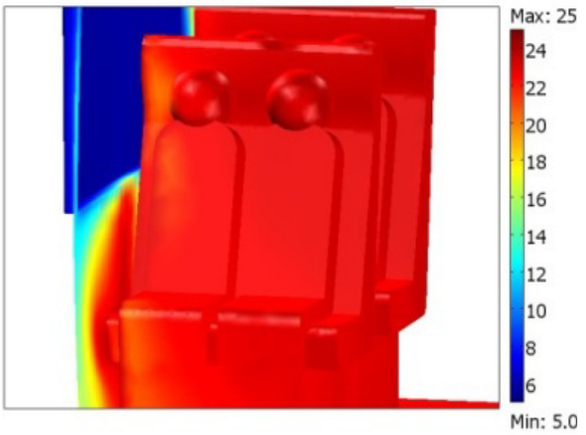

Figure 15. Temperature field at solid-fluid interfaces (MAD + UFD).

3.3. Hospital Isolation Room (IR): Influence of bio-effluent impulsively introduced by patients coughing

The third case study presented in this chapter concerns IAQ in a hospital IR. Analyses take into account the effect of patients' coughing on the indoor environment. Transient simulations were performed to investigate the efficiency of the existing HVAC plant with a Variable Air Volume (VAV) primary air system. Solid modelling of the room, taking into account thermo-physical properties of building materials, architectural features and furnishing arrangement of the room, inlet turbulence high induction air diffuser, the return air diffusers and two patients lying on two parallel beds was carried out. The 3D model of the room studied is provided in Figure 16.

The HVAC primary air system, designed for hospitalization infected patients, provides 6 m^3/h of inlet air and 7 m^3/h of extraction air. The room is ventilated by a commercial "turbulence" high induction air diffuser, located in the center of the ceiling and in the middle area between the two beds. The exhaust air is expelled by three return air diffusers located on the ceiling, the door of the toilet and the one adjacent to the corridor. The exhaust

vents of the ventilation system were set at an outlet pressure value in order to maintain the negative pressure within the room as imposed for infectious patients. The heads of the two patients lying on two parallel beds were modeled using solid geometry to take into account their different positions. In particular three outflow head surfaces were modeled and used to simulate the inlet surface of the bio-aerosols (mouth) related to the different position of each patient. The heads of the patients were also considered as two heat sources. Building thermal performances and thermo-physical properties of building envelope were taken into account. Three scenarios were investigated, which differ in the direction of coughing and breathing for the same position of the two patients, described by the "supine" position, the "face-to-face" position and the "back-to-back" position. Time dependent simulations were based on governing equations solution for the three scenarios with the aim of investigating the temporal patterns of the ventilation flow and the particles tracing and diffusion in the conditions of coughing and breathing of the two patients. The transient simulations with thermal and fluid-dynamic coupled models were preceded by a long enough run without cough/sneeze events in order to compute initialization states for transient simulations. Airflow pattern of steady solution and temperature field in the room were computed to define initial conditions for transient simulations. The sneeze and/or cough events were then considered at the beginning of the transient simulation.

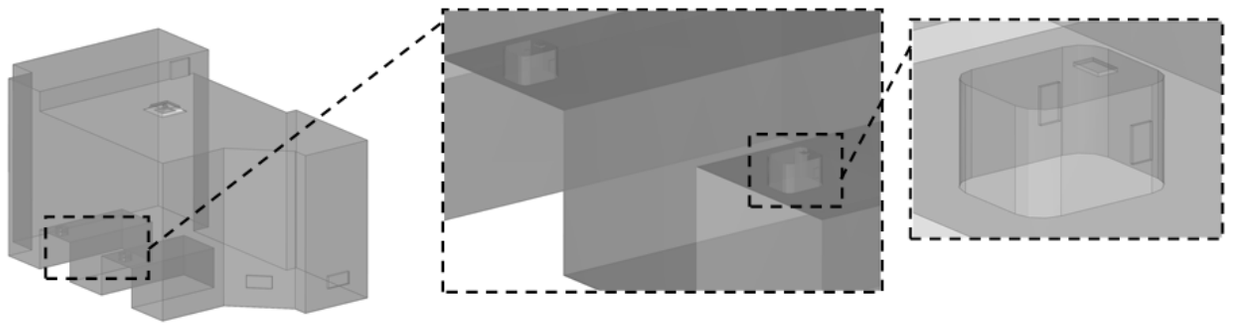

Figure 16. Outline of the geometrical system.

Then, considering each relative position between the patients, three events (coughing and/or breathing) were investigated: the first event (model_1) concerns the first patient coughing three times when the second is breathing; the second event (model_2) concerns the first patient coughing three times when immediately after the second coughs three times, the third (model_3) concerns both patients coughing, at the same time, three times. In particular for all the models the door was kept closed, so that particle diffusion would be influenced by ventilation airflow patterns alone. The "impulse" functions (volumetric and mass flow due to coughing) for the simulation of coughing events were repeated over time, with a time interval as "peak-to-peak" equal to 2 seconds. In model_2, the time phase displacement between coughing events of the two patients was taken as 6 seconds.

These conditions remain throughout the entire simulation of 60 seconds when the ventilation system operating and the coughing/breathing events happen. A peak of inlet

velocity value due to the cough was set at 28 m/s, which is the maximum experimentally determined connected to the transient flow due to the impulse that has a length of about one second. The inlet/outlet breathe velocity was considered constant 0.9 m/s. A particle tracing and diffusion model, connected to cough events, was developed to simulate the dispersal of bacteria-carrying droplets in the isolation room equipped with the existing ventilation system. An analysis of the region of droplet fallout and the dilution time of bacteria diffusion of coughed gas in the isolation room was performed.

The analysis of transient simulation results concerning particle path and distance, and then particle tracing combined with their concentration, provided evidence of the formation of zones that should be checked by microclimatic and contaminant control. Figure 17 reports, for model_2 (the first patient coughing three times when immediately after the second coughs three times) studied in the scenario called as “supine position”, an isosurface of aerosol concentration during first patient coughing. Figure 18 illustrated the same computed data for scenario “face-to-face”. For “supine position” of the patients the effluent concentration in the form of aerosol achieves the higher values in the time interval of 2-4 seconds and then decreases with time because the continuous dilution provided by the air flow inlet. For “face to face” position the effluent concentration, achieves the higher values in the same time interval, but during the transient air flow displacement a local effluent stagnation zone is produced between the two beds and small recirculation flows are generated near the patients due to lower displacement efficiency of the plant. For “overleaf to overleaf” position this effluent stagnation reaches intermediates values obtained from other two models. Particles tracing for the above cited analyses are also reported in figures 19-20 for “supine” and “overleaf to overleaf” scenarios . The particle tracing obtained from the models for the several scenarios simulations highlights the position during time of the particles due to cough with a diameter of 1E-5 m; the obtained trajectories are referred to those particles which position at the initial instant overlap with the surface of the mouth of the first coughing patient and the second breathing. Concerning the particle path and distance, for the “supine” position, during the first 10 seconds the particles go through about 1.8-1.9 meters along the orthogonal direction to the surface of the inlet air diffuser; in the final part of the transient analysis the particles trajectory, initially dependent on the inertial effect of the air throw, is influenced by the air ventilation outflow. For “face-to-face” position, during the first 10 seconds the particles go through about 1.6-1.7 meters along the orthogonal direction to the surface of the inlet air diffuser, then the particles flow due to the patient coughing can reach the face of the second patient. For the “overleaf-to-overleaf” position, in about four seconds the particles go through 1.4 meters along the orthogonal direction to the surface of the inlet air diffuser and then collide against the wall. Globally it can be observed as the potentially influenza viruses aerosolized could maintain the biological properties 24 hours if the humidity is 20%. The inactivation rate is about 1.69 day^{-1} on steel and 0.58 day^{-1} on linen, cotton and fabric fomites. From simulation results can be deduced as the stagnation zones could represent a source of infection when the rooms is used for different patients during the day.

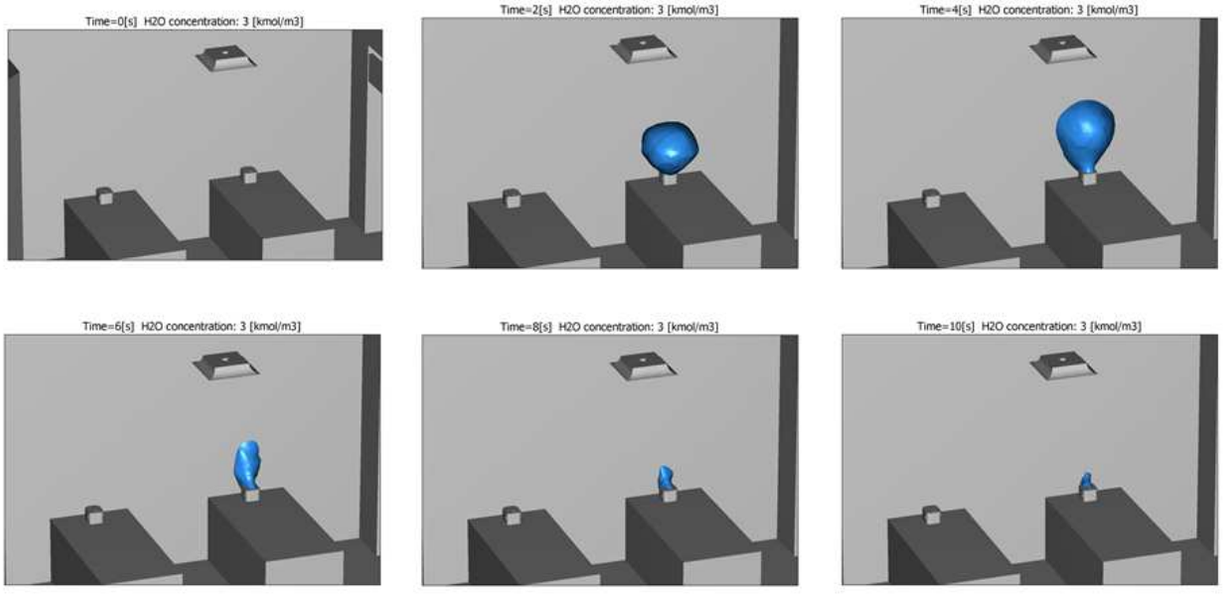

Figure 17. Isosurface of aerosol concentration for 1st patient coughing (model_2,"supine" scenario).

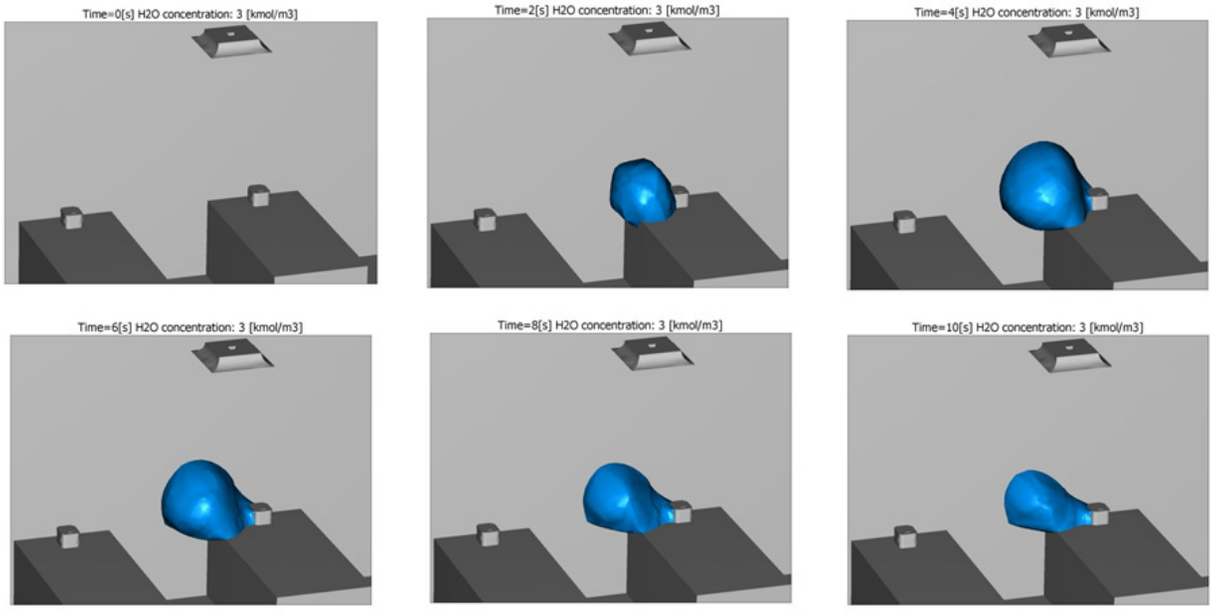

Figure 18. Isosurface of aerosol concentration for 1st patient coughing (model_2,"face-to-face" scenario).

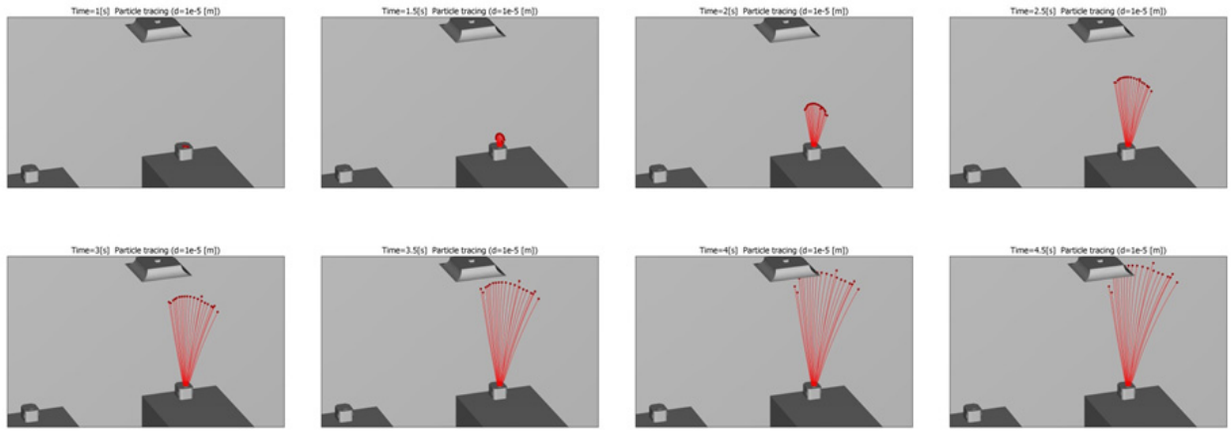

Figure 19. Particle tracing for aerosol during first patient coughing (model_2,"supine" scenario).

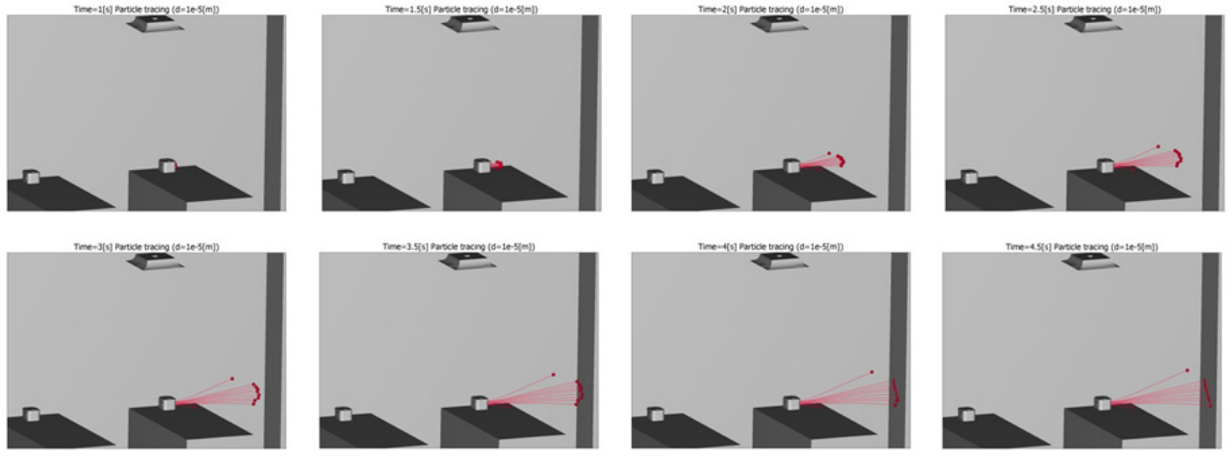

Figure 20. Particle tracing for aerosol during first patient coughing (model_2,"back-to-back" scenario).

3.4. Hospital Operating Theatre (OT): Influence of door opening/closing and people moving

The last presented application is devoted to investigate on IAQ in a OT keeping into account effects due to the opening/closing of a sliding door and the medical staff movement when crossing the open door-space. Transient simulations were performed for three cases:

a. Opening and closing of the sliding door (Case A);
b. Opening of the sliding door, one person crossing, closing of the sliding door (Case B);
c. Opening of the sliding door, two persons with a stretcher crossing, closing of the sliding door (Case C).

The physical and architectural model of the OT was based on a typical and standard layout of the ISO5 class with ultra clean air filters system. The operating room is 6.3 m wide, 6.3 m long with a total volume of 119.07 m^3. We referred to a HVAC plant systems that meets the most important standard requirements. The functional and operating parameters of the HVAC system with primary air unit and a ceiling unidirectional diffuser are provided in Table 3.

Air ceiling unidirectional inlet diffuser		
Effective surface (> 90% of the floor area)	36	[m^2]
ACH (Air Change per Hour)	200	[1/h]
Minimum air change flow rate	1500	[m^3/h]
Mean inlet velocity adopted	0.184	[m/s]
Minimum over-pressure differential	5	[Pa]

Table 3. Functional and operating parameters of HVAC system.

The internal air temperature of the OT was set at 20 °C and that of the surrounding zones at 26 °C as suggested. Taking into account literature suggested values [33] for a standard ISO5 class operating room, furniture, basic safety lighting systems, surgical lighting surgical staff position were disregarded but thermal power provided were considered: the total thermal power released by 8 persons was taken a 920 W, for general lighting 400 W and for surgical equipment 1 kW. The sliding door clear opening of the OT is 900 mm x 2100 mm with a thickness of 40 mm, representative of a door made by an aluminum frame and a galvanized steel sheet panel. The geometry of the studied system is outlined in Figure 21.

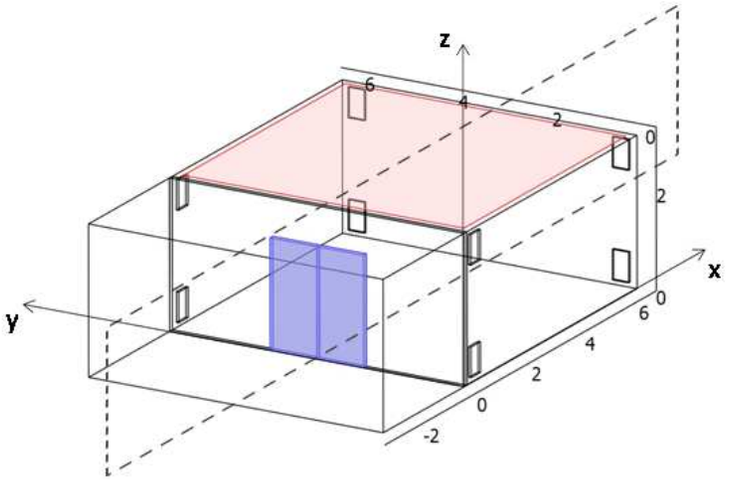

Figure 21. Geometry of the outlined OT and representation of the "zx" symmetry plane (dashed lines) considered for studying one half of the system.

The operating room is accessible from a 3 m breadth adjacent corridor by a two-panels sliding door, represented in blue in Figure 21. As introduced, the considered room is equipped by specific air vents and recovery grids in order to assure an unidirectional flow inside the hall. The air diffuser covers almost all the ceiling surface, extending for 6 m x 6 m over the room (pink surface in Figure 21). The recovery grids are located at the top and at the bottom corners of the room. Exploiting the geometrical symmetry of the system with respect to the mid zx-plane, one half of the presented system was considered in computations. In order to validate this assumption some preliminary tests were carried-out by considering the full geometry of the system. No important differences in test results have been remarked between the full model and the one-half model of the considered OT.

3.4.1. Implemented procedure for "moving objects" simulation

The adopted procedure in order to simulate the solid objects moving in the fluid domain is mainly based on the definition of specific source terms in the above reported governing equations (1-5), assuming assigned values in the portions of the computational domains where the solid objects are located at a chosen time. Moving of interfaces describing the position of the solid object, that are not explicitly designed in the geometrical models, is driven by some logical functions preliminarily defined, that allow simulating of the dynamics associated with the sliding door opening/closing and persons walking across the OT. The procedure mainly consists in defining some logical functions assuming binary values that identify the portions of domain where solid objects are located (binary value 1) or not (binary value 0) at the initial time. The binary value assumed by the logical functions depends on assigned geometrical coordinates for each object. In those regions fluid-dynamical properties and source terms assume specific values determining rest conditions for fluid. Time-dependent functions allow modification of the geometrical coordinates identifying the position of the "solid" objects during time, so that a prescribed motion law can be assigned to the moving objects. Let us first consider the door as example of the applied procedure. The following expressions have been used to define its spatial coordinates:

```
x1_door = x10_door
x2_door = x20_door
y1_door = y10_door
y2_door = y20_door-func_dy(t)
z1_door = z10_door
z2_door = z20_door
```

A graphic representation is given in Figure 22 to better elucidate the meaning of the above reported expressions. In this figure the solid objects (door outlined in pink and persons/litter in blue) are geometrically represented only for the sake of clarity, these geometries in fact are not really outlined in the numerical models used for computations. The above expressions assume constant or variable values in time. The time-function `func_dy(t)` denotes the motion law assigned to the door in the y direction (constant sliding velocity equals 0.66 m/s). When `func_dy` assumes the value "0" the door is closed, otherwise, when the assumed value is "1" the door is completely open (the door width being 1 meter). The following logical functions have been then defined in order to identify the coordinates' range, along each axis, identifying the door position:

```
x_door = if ((x>x1_door)and(x<x2_door)) then 1 else 0
y_door = if ((y>y1_door)and(y<y2_door)) then 1 else 0
z_doo = if ((z>z1_door)and(z<z2_door)) then 1 else 0
```

Position of the solid object "door" analytically corresponds to value "1" assumed by the following expression:

```
door = x_door*y_door*z_door
```

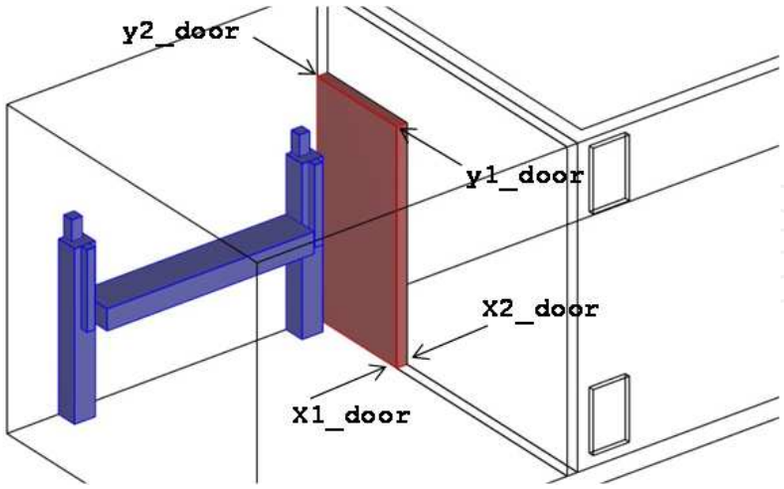

Figure 22. Expressions used to characterise positions of the "solid objects".

The same procedure is applied for defining position of the other "solid objects" (head, harms and body for each person and litter) during time. In this case, a second motion law (`func_dx(t)`) is defined in order to simulate the person and stretcher movements along the x-direction throughout the free door-space once the door is open. The constant advancing velocity chosen for the person is 0.84 m/s. Time evolution of the functions applied to define the passage of the "solid objects" for the different simulated case studies reported in this paper are graphically reported in Figure 23. Due to its formulation, the present numerical procedure can be applied to prismatic solid objects only. Once the solid object position is defined during time, some further functions could be used for assigning physical properties to these portions of the numerical domain, as given below:

```
eta_dom = if((door>0)or(P#1>0)or(P#2>0)or(L>0)) then eta_solid else
eta_fluid
rho_dom = if((door>0)or(P#1>0)or(P#2>0)or(L>0)) then rho_solid else
rho_fluid
k_dom = if((door>0)or(P#1>0)or(P#2>0)or(L>0)) then k_solid else
k_fluid
Cp_dom = if((door>0)or(P#1>0)or(P#2>0)or(L>0)) then Cp_solid else
Cp_fluid
```

where expressions `P#1`, `P#2` and `L` relate to person 1, person 2 and stretcher and, in analogy with expression door used for the door, they identify the people and stretcher position where their value is "1". It should be noticed that this procedure makes it possible to use average values of the physical properties for all the solid objects only. This does not represent an inconvenience for viscosity in the momentum equations, as its value is chosen arbitrarily high (1E+5) in order to contribute to motion enabling.

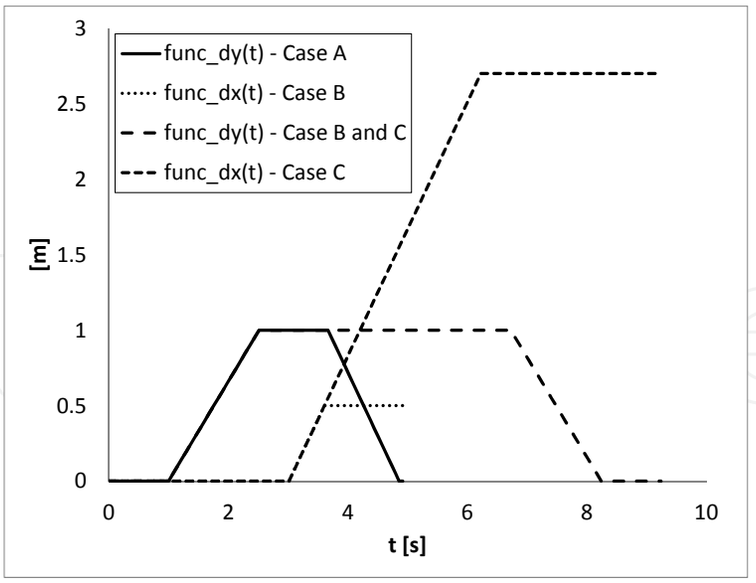

Figure 23. Functions defining the "solid objects" dynamics.

Otherwise, the use of an average value of density, thermal conductivity and thermal capacity in the energy equation should be verified by specific test cases. During the present study we compared steady solutions obtained by solving a model based on a classical implementation of the solid objects (partially opened position for the door) and a model based on the discussed here modelling procedure. Comparison has shown very low difference in temperature profiles, especially in airflow behaviour, that is the main point of modelling method proposed in this study. Numerical values used for physical properties in "fluid" and "solid" domains are listed in Table 4, where values used for the partition wall facing the corridor are also given.

	S.I Unit	"Fluid"	"Solid"	Wall
ϱ	[kg/m^3]	1.2	900	600
η	[Pa s]	5E-5	1E+5	-
k	[W/(m K)]	0.62	0.6	0.16
C_p	[J/(kg K)]	1004	2000	840

Table 4. Numerical values of constants used in the adopted mathematical model.

Therefore, some special sources terms have been implemented in the governing equations. In order to enable motion in the solid objects, we defined:

```
S_dom = if((door>0)or(P1>0)or(P2>0)or(L>0)) then 0 else 1
F_dom = (C*(1-S_dom)^2)/(S_dom^3+ES)
```

Being C=1.6E+6 and ES=1E-4 constant values [43]. Note that F_dom becomes null where S_dom=1 (volume of fluid). In order to enable thermal transport in solid objects, in the energy equation we defined the components of thermal transport vector as follows:

```
u_dom = if((door>0)or(P#1>0)or(P#2>0)or(L>0))then 0 else u
v_dom = if((door>0)or(P#1>0)or(P#2>0)or(L>0))then 0 else v
```

```
w_dom = if((door>0)or(P#1>0)or(P#2>0)or(L>0))then 0 else w
```

being u, v ,w the components of the velocity vector. Finally, in order to consider the metabolic heat produced by people, we considered the following source term in the energy equation:

```
Q_dom = if((P#1>0)or(P#2>0))then Q else 0
```

Metabolic rate was assumed to be 2 Met (walking person), that corresponds to a specific heat source Q_dom = 1300 W/m^3.

3.4.2. Transient results

Figure 24 presents the velocity field and the velocity vectors in a horizontal slice of the OT (1.5 meters from the floor) during the door opening in the Case A.

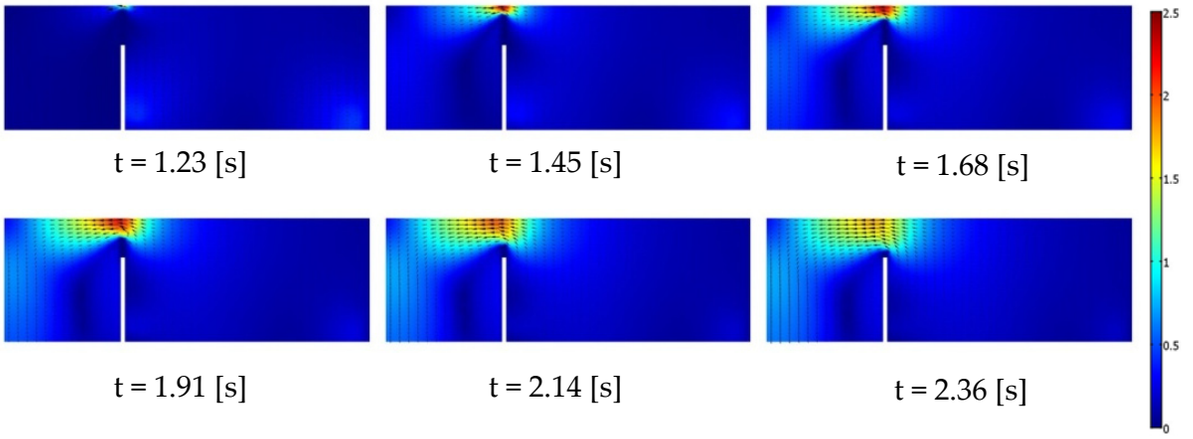

Figure 24. Velocity field [m/s] and velocity vectors in a horizontal plane (z = 1.5) at several time instants during the door opening (Case A).

Due to the pressure level inside the OT, a flow rate of air from the room to the corridor is highlighted when the door opens. The maximum magnitude of the flow velocity is reached for a partial opening position of the door. As a matter of fact, Figure 25 shows, for several time instants, the x-velocity profiles along the y-direction in correspondence of the door-space (line represented in red in the figure, lying at 1 meter from the floor). The negative values assumed by the x-velocity component depend by the chosen orientation of the Cartesian system of coordinates, and well underline the air flow direction when the door is opening. This effect, caused by the mixing between the air flow inside the room with that at the ceiling supply diffuser and the outside flow, is confirmed by recent studies [32]. The effect of temporal or extended period of door opening but also of surgical staff movements, that can obstruct the ventilation system efficiency, widely explained in the above cited papers, can be compared with our simulation results connected to relative velocity and pressure difference variations. In particular our obtained results can be strongly compared with those concerning the work of Brohus et al. [38] on the influence of person movements on contaminant transport in an operating room evaluated by smoke visualization and CFD

simulations. As a matter of fact the effects we found on the velocity distribution and pressure variations due to persons and sliding door movements through the LAF field are very similar. A similar way of representation used in Figure 25 is applied in Figure 26-27 to report results obtained for Case B and Case C. Figure 26 refers to Case B and presents the velocity magnitude computed along a line lying along the x-direction (red line in figure, y=3.05, z=1.5) for several time instant during the person crossing of the open door. As can be appreciated, velocity achieves null value in the x-range corresponding to the person position during the door-space crossing. Similar considerations can be pointed-out by looking at Figure 27, that refers to Case C simulation. In this case the x-range where velocity magnitude is zero is much wider, because of the presence of two persons and a transported stretcher crossing the door-space. In confirmation, Figure 28 presents for the Case C the velocity magnitude evaluated along a x-directed line (red in the figure) lying at a distance from the floor higher than the stretcher one. In that figure two zero x-ranges can be appreciated, that correspond to the position, at each time step, of the two persons. Figure 29 collects some pictures referring to Case C, reporting the velocity fields in a longitudinal section of the OT (y=3.05) during the persons/stretcher crossing of the door-space. They highlight the "solid objects" moving across the door-space, from the corridor to the OT. The air distribution is significantly perturbed by the persons/stretcher incoming inside the OT, that involves in local airstream from the OT to the corridor, reaching values of velocity magnitude up to 1.5 m/s.

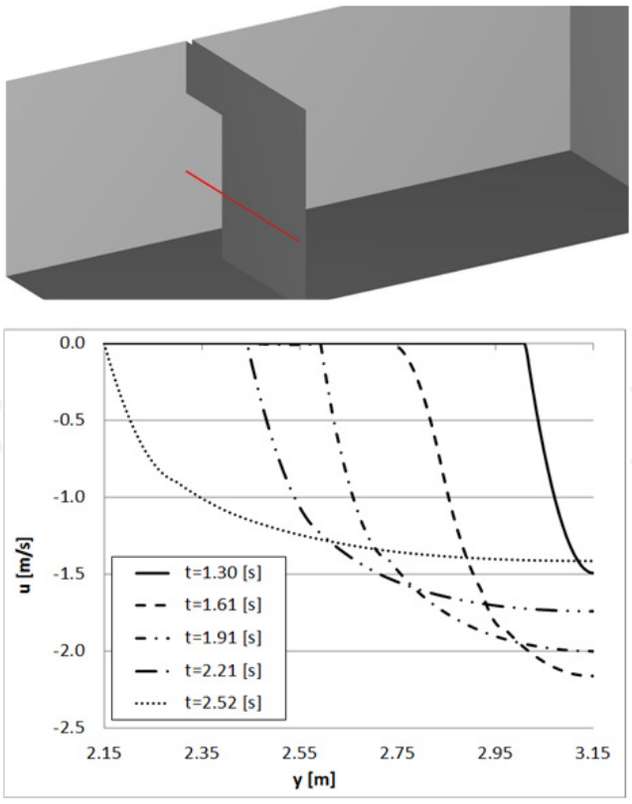

Figure 25. Velocity component u along a y-lying (z = 1 and x = 0) for several time instants during the door opening (Case A).

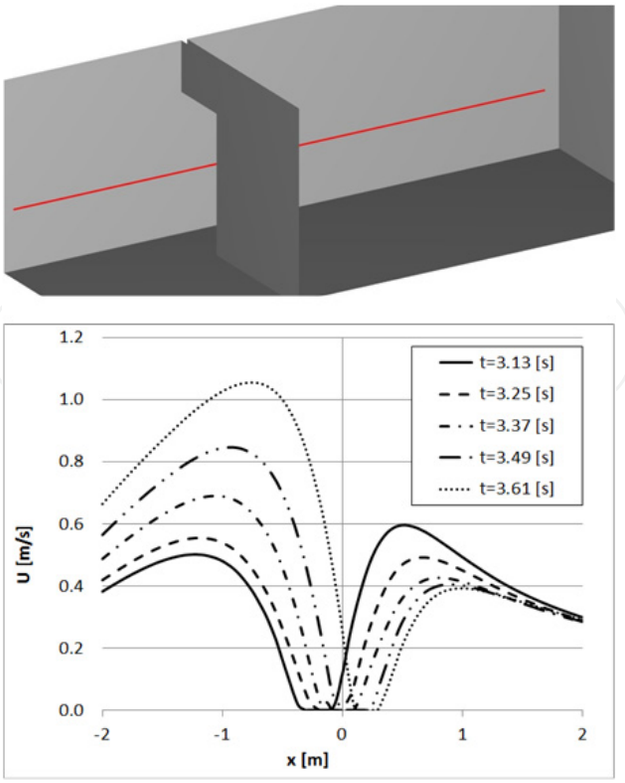

Figure 26. Velocity magnitude along a x-lying (z = 1 and y = 3.05) for several time instants during the person crossing (Case B).

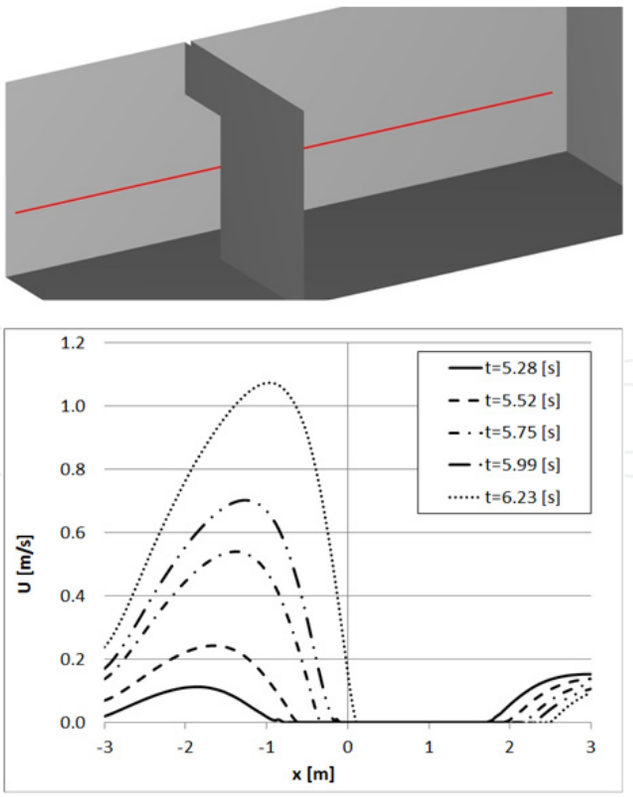

Figure 27. Velocity magnitude along a x-lying (z = 1 and y = 3.05) for several time instants during the persons and stretcher crossing (Case C).

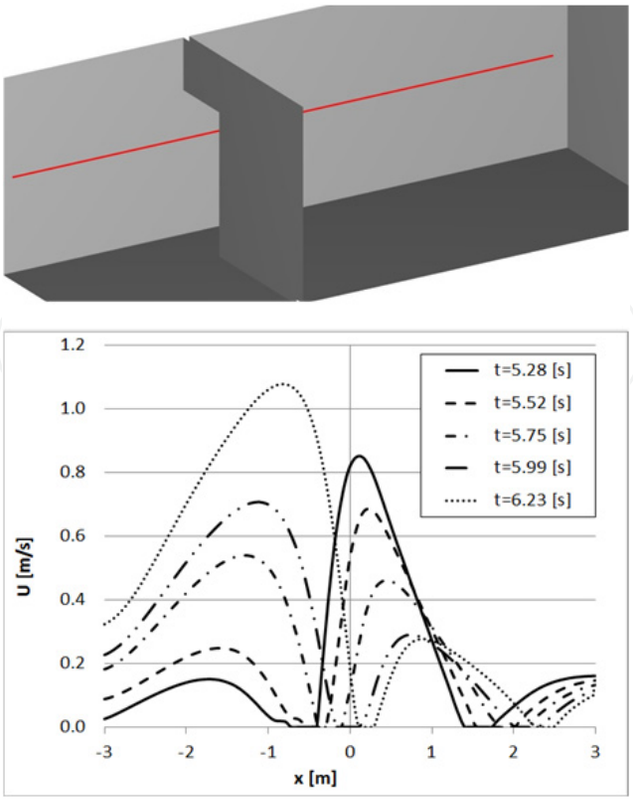

Figure 28. Velocity magnitude along a x-lying (z = 1.5 and y = 3.05) for several time instants during the persons and stretcher crossing (Case C).

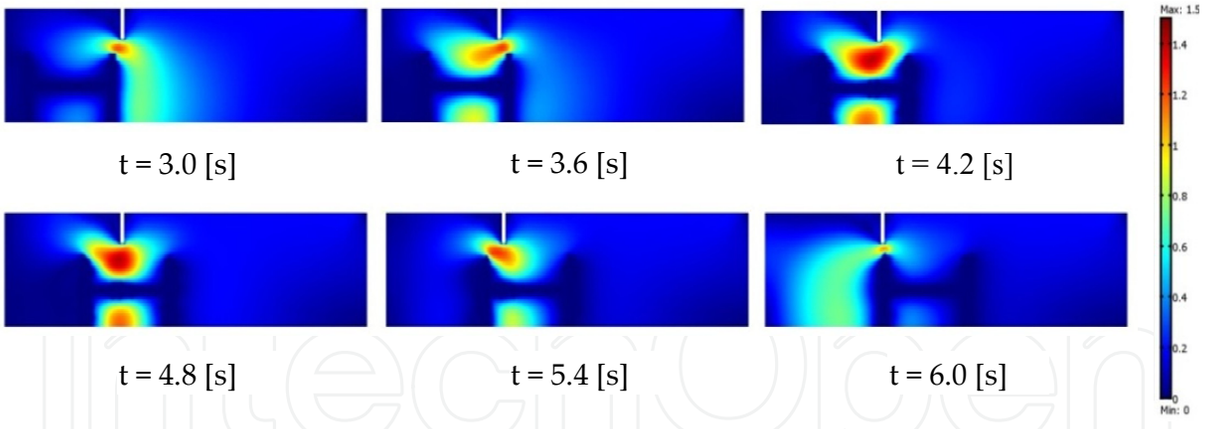

Figure 29. Velocity field [m/s] in a vertical plane (y = 3.05) at several time instants during the persons/stretcher crossing (Case C).

4. Conclusion

This chapter presents several case studies concerning multi-physical simulation for IAQ monitoring in internal environments with high crowding level and/or risk of contamination. A brief description on mathematical and numerical schemes adopted for carrying-out simulation results leads up to the chapter main body, where four real-world applications are presented and discussed. The first one is devoted to investigate on the influence of the air-

distribution layout on IAQ and thermal comfort in a movie theatre hall. From results some interesting items can be remarked. When MAD system is applied a potential draught effect could be perceived by some of the spectators, depending on their place. That condition is increased for PAD system. Otherwise, the UFD system guarantees a better level of comfort from this point of view. From thermal analyses it appears that UFD system assures the most homogeneous thermal field, while PAD system generates disagreeable conditions related to high temperature gradients in the occupied zone. Authors are carrying out some three-dimensional simulations in order to better elucidate this finding. Referring to carbon dioxide level in the occupied zone, the PAD system is otherwise detected to be better than MAD and UFD ones, assuring a higher dilution of the bio-effluent with respect to the other systems. Anyway, the air stream determined by the personalized ventilation allows air breathed out by a person to be potentially transferred to the person seated in the rear row. This item could become critical because of a potential risk of contamination. From the air "freshness" point of view, the MAD is surely the worst system among the studied ones. The diffusers location, at the ceiling level, determinates very high values of the mean age of air supplied to spectators with respect to PAD and UFD layouts. The aim of the second case study presented in very similar to the that refers to the first one. In this last case we investigated on IAQ inside cabins of means of transportation depending on the applied layout for ventilation air distribution. The goal was to strike a balance between air quality degradation and comfort conditions for passengers standing in an aircraft cabin potentially equipped by three kinds of air distribution system. Results mainly show as from the comfort condition the most appropriate system is the UFD system. In fact it assure the lower velocity level close to the passenger's face. From the air quality point of view, the PAD system represent instead the best choice because it allows very low level of stagnant bio-effluent close to the passenger's nose. Anyway, referring to the contamination risk inside the cabin, this system is detected to be the most critical because it allows particle breathed out by a passenger to be potentially inhaled by another. Globally it appears that in absence of relevant challenges to be pursued in the most recent UFD and PAD systems, the classical MAD represent the better compromise between opposite requirements. The third application concerns the effect of patients coughing in a hospital isolation room and the performance of the HVAC system in diluting the bio-effluents introduced in the indoor environment. Results indicate the best conditions for the high induction air inlet diffuser and the scheme of pressures imposed in the room to provide the effective means of controlling flows of virus-loaded droplets. Our findings stress that the position of the air-supply inlets in the ceiling and the exhaust vents at the opposite side of the room and in the ceiling, provide an up-draft effect and infection control efficiency. When the air-supply inlet is located in the middle of the ceiling of the room, and the exhaust vents are positioned in the wall behind the patient beds, the coughed particles and gas are contained at the side of the patient in the region of the exhaust vents. This can minimize the region of coughed gas diffusion and droplet fallout. The high induction air inlet diffuser and the scheme of pressures imposed in the room provide the effective means of controlling droplet flows containing viruses. This type of analysis allows to predict air recirculation zones which can host pathogens. Indeed our analysis of the particle tracing and path distribution combined with their concentration, was effective in

identifying examples of such zones between the two beds, around the ceiling surface and on the surface of the bed lamps. The last case study is devoted to IAQ investigation in a hospital operating room, taking into account the sliding door and the medical staff movements. The study provides a simplified indirect numerical method to simulate the influence of solid objects movement, that exploits analytical expressions to dynamically track the solid-fluid interfaces in the computational domain. Special source terms were implemented in the governing equations in order to enable air-flow in domain's portions where solid objects are located at a chosen time. The used turbulence method was preliminary validated by comparing numerical results with experimental data available in literature for similar cases. Results, obtained for the three cases studied, highlight a strong modification of the air velocity field inside the OT, due to opening/closing door and staff movements. Air leakages through the door clear-space were estimated for each configuration. The air-flow rates, coming out the OT under transient conditions, were also correlated to the HVAC energy overload. An important reduction of the overpressure assured by the HVAC system inside the studied room was clearly evaluated, highlighting that pressure reaches values very close to the minimum threshold limits recommended by the most important international standards concerning the OT climate conditions. We are persuaded that the proposed numerical approach, based on FE multi-physical analysis in order to investigate on IAQ, can be reputed as a powerful and reliable tool to be used for the comprehension and analysis of the airflow and pressure distribution in several class of applications. For that reason, we believe that the introduction of the practice of performing multi-physical simulations on real cases will be an effective, relatively low cost, means of prediction and control.

Author details

Giuseppe Petrone* and Giuliano Cammarata
Department of Industrial Engineering, University of Catania, Catania, Italy

Carla Balocco
Energy Engineering Department, University of Firenze, Firenze, Italy

5. References

[1] Fanger PO (1970). Thermal comfort. Copenhagen: Danish Technical Press.
[2] Fanger PO (1988a). Introduction of the olf and the decipol units to quantify air pollution perceived by humans indoors and outdoors. Energy and Buildings, 12: 1-6.
[3] Awbi HB (2003). Ventilation of buildings. London: Spon Press, Taylor & Francis Group.
[4] Alamari F, Butler DJG, Grigg PF, Shaw MR (1998). Chilled ceilings and displacement ventilation. Renewable Energy, 15: 300-305.
[5] Fredriksson J, Sandberg M, Moshfegh B (2001). Experimental investigation of the velocity field and airflow pattern generated by cooling ceiling beams. Building and Environment, 36: 891-899.

* Corresponding Author

[6] Zhang L, Chow TT, Fog KF, Tsang CF, Qiuwang W (2005). Comparison of performances of displacement and mixing ventilations. Part II: indoor air quality. International Journal of Refrigeration, 28: 288-305.

[7] Fleming WS (1986). Indoor air quality, infiltration, and ventilation in residential buildings. In Proceedings of: ASHRAE Conference IAQ'86: Managing Indoor Air for Health and Energy Conservation, Atlanta, GA, USA; pp. 192–207.

[8] Persily A (1997), Evaluating building IAQ and ventilation with indoor carbon dioxide. ASHRAE Trans, 103: 193–204.

[9] Daisey JM, Angell WJ, Apte MG (2003). Indoor air quality, ventilation and health symptoms in schools: an analysis of existing information. Indoor Air, 13: 53-64.

[10] Papakonstantinou KA, Kiranoudis CT, Markatos NC (2002). Numerical simulation of CO2 dispersion in an auditorium. Energy and Buildings, 200: 245–250.

[11] Cheong KWD, Lau HYT (2003). Development and application of an indoor air quality audit to an air-conditioned tertiary institutional building in the tropics. Building and Environment, 38: 605-616.

[12] Cheong KWD, Djunaedy E, Chua YL, Tham KW, Sekhar SC, Wong NH, Ullah NB (2003), Thermal comfort study of an air-conditioned lecture theatre in tropics. Building and Environment, 38: 63–73.

[13] Noh KC, Jang JS, Oh MD (2007). Thermal comfort and indoor air quality in the lecture room with 4-way cassette air-conditioner and mixing ventilation system. Building and Environment, 42: 689-698.

[14] Kavgic M, Mumovic D, Stevanovic Z, Young A (2008). Analysis of thermal comfort and indoor air quality in a mechanically ventilated theatre. Energy and Buildings, 40: 1334-1343.

[15] Wang A, Zhang Y, Sun Y, Wang X (2008) Experimental study of ventilation effectiveness and air velocity distribution in an aircraft cabin mockup, Building and Environment, 43, 337-343.

[16] Petrone G, Cammarata L, Cammarata G (2011). A multi-physical simulation on the IAQ in a movie theatre equipped by different ventilating systems, Building Simulation, 4: 21-31.

[17] Arens E, Xu T, Miura K, Zhang H, Fountain M, Bauman F (1998). A study of occupant cooling by personally controlled air movement. Energy and Buildings, 27: 45–49.

[18] Demetriou DW, Khalifa HE (2009). Evaluation of distributed environmental control systems for improving IAQ and reducing energy consumption in office buildings. Building Simulation, 2: 197-214.

[19] Niu J, Gao N, Phoebe M, Huigang Z (2007). Experimental study on a chair-based personalized ventilation system. Building and Environment, 42: 913-925.

[20] Bauman F (2003). Underfloor Air Distribution (UFAD) Design Guide. American Society of Heating, Refrigerating, and Air Conditioning Engineers Research Project RP-1064. Atlanta.

[21] Zhang T, Chen QY (2007). Novel air distribution systems for commercial aircraft cabins. Buildings and Environment, 42: 1675-1684.

[22] Tang J, Li Y, Eames I, Chan P, Ridgway G (2006). Factors involved in the aerosol transmission of infection and control of ventilation in healthcare premises. Journal of Hospital Infection, 64: 100-114.
[23] Zhao B, Yang C, Chen C, Feng C, Yang X, Sun L, Gong W, Yu L (2009). How Many Airborne Particles Emitted from a Nurse will Reach the Breathing Zone/Body Surface of the Patient in ISO Class-5 Single-Bed Hospital Protective Environments? A Numerical Analysis. Aerosol Science and Technology, 43: 990–1005.
[24] Talon D, Schoenleber T, Bertrand X, Vichard P (2006). Performances of different types of airflow system in operating theatre. Annales de Chirurgie 131: 316-321.
[25] Balocco C, Lio P (2011). Assessing ventilation system performance in isolation rooms. Energy and Buildings, 43:246-252.
[26] Balocco C (2011). Hospital ventilation simulation for the study of potential exposure to contaminants. Building Simulation, 4: 5-20.
[27] Tunga YC, Hu SC, Tsai TI, Chang IL (2009). An experimental study on ventilation efficiency of isolation room. Building and Environment, 44: 271-279.
[28] Chow TT, Kwan A, Lin Z, Bai W (2006b). Conversion of operating theatre from positive to negative pressure environment, Journal of Hospital Infection, 64: 371-378.
[29] Menazadeh F, Manning AP (2002). Comparison of Operating Room ventilation systems in the protection of surgical site. ASHRAE Transactions, 108: 1-13.
[30] Chow TT, Yang XY (2004). Ventilation performance in operating theatres against airborne infection: review of research activities and practical guidance. Journal of Hospital Infection, 56: 85–92.
[31] Dong S, Tu G, Cao R, Yu Z (2009). Numerical Study on Effects of Door-Opening on Airflow Patterns and Dynamic Cross-Contamination in an ISO Class 5 Operating Room. Trans. Tianjin University, 15: 210-215.
[32] Shih YC, Chiu CC, Wang O (2007). Dynamic airflow simulation within an isolation room. Building and Environment, 42: 3194–3209.
[33] Matzumoto H, Ohba Y (2004). The Influence of a Moving Object on Air Distribution in Displacement Ventilated Rooms, Journal of Asian Architecture and Building Engineering, 3: 71-75
[34] Halvonovà B, Melikov AK (2010). Performance of ''ductless'' personalized ventilation in conjunction with displacement ventilation: Impact of disturbances due to walking person(s). Building and Environment, 45: 427–436.
[35] Balocco C, Petrone G, Cammarata G (2012). Assessing the effects of sliding doors on an operating theatre climate. Building Simulation, 5:73-83.
[36] Brohus H, Balling KD, Jeppesen D (2006). Influence of movements on contaminant transport in an operating room. Indoor Air, 16: 356-372.
[37] Wilcox DC (1998), Turbulence Modelling for CFD, DCW Industries Inc.
[38] Abanto J, Rarrero D, Reggio M, Ozell B (2004). Air flow modelling in a computer room. Building and Environment, 39: 1393-1402.
[39] Zhang L, Chow TT, Fog KF, Tsang CF, Qiuwang W (2005). Comparison of performances of displacement and mixing ventilations. Part II: indoor air quality. International Journal of Refrigeration, 28: 288-305.

[40] Deuflhard P (1974). A modified Newton method for the solution of ill-conditioned systems of nonlinear equations with application to multiple shooting. Numerical Mathematics, 22: 289-315.
[41] Hindmarsh AC, Brown PN, Grant KE, Lee SL, Serban R, Shumaker DE, Woodward CS (2005). SUNDIALS: Suite of Nonlinear and Differential/Algebraic Equation Solvers. ACM Transactions on Mathematical Software, 31: 363-396.
[42] Fanger PO, Melikov A, Hanzawa H, Ring J (1988b). Air turbulence and sensation of draught. Energy and Buildings, 12: 21-39.
[43] Debabrata P, Yogendra KJ (2001). Melting in a side heated tall enclosure by a uniformly dissipating heat source. International Journal of Heat and Mass Transfer, 44: 375-387.